Hindawi Publishing Corporation
Advances in High Energy Physics
Volume 2013, Article ID 505874, 18 pages
http://dx.doi.org/10.1155/2013/505874

Review Article

Neutrinoless Double β^+/EC Decays

Jukka Maalampi and Jouni Suhonen

Department of Physics, University of Jyväskylä, P.O. Box 35 (YFL), Jyväskylä 40014, Finland

Correspondence should be addressed to Jouni Suhonen; jouni.suhonen@phys.jyu.fi

Received 28 June 2013; Accepted 19 September 2013

Academic Editor: Srubabati Goswami

The relation of neutrino masses to neutrino oscillations and the nuclear double beta decay is highlighted. In particular, the neutrinoless $\beta^+\beta^+$, β^+EC, and resonant ECEC decays are investigated using microscopic nuclear models. Transitions to the ground state and excited 0^+ states are analyzed. Systematics of the related nuclear matrix elements are studied and the present status of the resonant ECEC decays is reviewed.

1. Introduction

The modern neutrino oscillation experiments have brought the study of neutrino properties to the era of precision measurements. At the same time the fundamental character (Majorana or Dirac) of the neutrino is still unknown, as is also its absolute mass scale. To gain information on these two unknowns the atomic nuclei can be engaged as the mediators of the Majorana-neutrino triggered neutrinoless double beta ($0\nu2\beta$) decays. The key issue here is how to cope with the involved nuclear-structure issues of the decays, crystallized in the form of the nuclear matrix elements (NMEs) [1–3]. To be able to exploit the potential data extracted from the $0\nu2\beta$-decay experiments one needs to evaluate the NMEs in a reliable enough way. It has become customary to employ the neutrino-emitting correspondent of $0\nu2\beta$ decay, the two-neutrino double beta ($2\nu2\beta$) decay, to confine the nuclear-model degrees of freedom in the NME calculations. The $2\nu2\beta$ decay is a second-order process in the standard model of the electroweak interactions and the associated half-lives have been measured for several nuclei [4].

The neutrinoless double β^- ($0\nu\beta^-\beta^-$) decays have been studied intensively over the years [2, 3] due to their favorable decay Q values. The positron-emitting modes of decays, $\beta^+\beta^+$, β^+EC, and ECEC, are much less studied. From here on we will denote all these decay modes as $0\nu\beta^+$/EC decays. The general, nuclear model independent frameworks of theory for these decays have been investigated in [7] for the $0\nu\beta^+$/EC-decay channels $\beta^+\beta^+$ and β^+EC. The formalism for the resonant neutrinoless double electron capture (R0νECEC) was first developed in [8] and later discussed and extended to its radiative variant ($0\nu\gamma$ECEC) in [9]. Due to the resonant nature of the R0νECEC decay its studies have called for precise measurements of the mass differences of the atoms involved in the decays. The resonant mode of 0νECEC decays is studied intensively for its potential enhanced sensitivity to discover the Majorana mass of the neutrino and that is why much experimental effort is being invested in observing this mode of decay.

2. Neutrino Masses and Oscillations

In the calculations of transition rates of the $0\nu\beta^+$/EC decays, the neutrino-physics part and nuclear-physics part factorize. We will start by considering the neutrino-physics part. The weak-interaction Lagrangian of leptons is diagonal in the neutrino fields ν_e, ν_μ, and ν_τ, called flavor eigenfields. The charged-current interaction part of the Lagrangian of the Standard Model of electroweak interactions, which is relevant to the considerations of this presentation, is given by

$$\begin{aligned}\mathcal{L}_{CC} &= -\frac{g}{2\sqrt{2}}\sum_{\ell}\overline{\nu}_{\ell}\gamma_{\mu}\left(1-\gamma_5\right)\ell W^{\mu} + \text{h.c.}\\ &= -\frac{g}{\sqrt{2}}\sum_{\ell}\overline{\nu}_{\ell L}\gamma_{\mu}\ell_L W^{\mu} + \text{h.c.},\end{aligned} \tag{1}$$

where ℓ refers to the three lepton flavors, $\ell = e, \mu, \tau$, W^μ is a vector field corresponding to the charged weak boson $W^\pm$, $\nu_{\ell L}$ and ℓ_L are the left-handed chiral components of the neutrino and charged lepton fields, and g is the gauge coupling constant. In all phenomena studied so far neutrinos appear as ultrarelativistic particles, but it is known that, albeit being extremely light compared with other fermions, neutrinos do have mass, evidenced by observations of many neutrino-flavor-oscillation phenomena (see, e.g., [10–18]). In neutrino oscillations transitions between neutrino flavors take place, indicating that neutrinos mix with each other. This mixing arises through the mechanism that gives neutrinos their mass. The mass part of the neutrino Lagrangian is hence not diagonalized by the flavor fields ν_ℓ but by fields ν_i ($i = 1, 2, 3$) that have definite masses m_i, known as the mass eigenfields. The left-handed flavor eigenfields appearing in the interaction Lagrangian (1) are superpositions of the left-handed components of the mass eigenfields:

$$\nu_{\ell L} = \sum_{\ell = e,\mu,\tau} U_{\ell i} \nu_{iL}, \tag{2}$$

where U is a unitary 3×3 matrix, called the neutrino mixing matrix or Pontecorvo-Maki-Nakagawa-Sakata (PMNS) matrix [19, 20].

The mass of the left-handed neutrinos can arise from mass terms of the form

$$-\frac{1}{2} M^L_{\ell\ell'} \overline{(\nu_{\ell L})^C} \nu_{\ell' L} + \text{h.c.}, \tag{3}$$

the so-called Majorana mass terms. They can arise in the Standard Model of particle physics through nonrenormalizable interactions between neutrinos and neutral Higgs bosons: $-(Y_{\ell\ell'}/\Lambda)\overline{(\nu_{\ell L})^C}(H^0)^2 \nu_{\ell' L}$ + h.c., where $Y_{\ell\ell'}$ is the Yukawa coupling constant, Λ is the energy scale of some new physics not present in the Standard Model, and H^0 is a neutral Higgs field. In the Standard Model, the vacuum expectation value of the neutral Higgs field is nonzero, $\langle H^0 \rangle = v/2 \neq 0$, giving rise to the following Majorana mass term for the left-handed neutrinos:

$$-\frac{v^2 Y_{\ell\ell'}}{4\Lambda} \overline{(\nu_{\ell L})^C} \nu_{\ell' L} + \text{h.c.}, \tag{4}$$

that is, $M^L_{\ell\ell'} = v^2 Y_{\ell\ell'}/2\Lambda$.

One assigns leptons an additive quantum number called the lepton number L, such that $L = +1$ for particles and $L = -1$ for antiparticles. The lepton number is conserved in the standard electroweak interactions, like in the charged-current interactions described by the Lagrangian (1), but the Majorana mass term (3) breaks it by two units; that is, Majorana mass terms are sources or sinks of the lepton number. No empirical evidence of nonconservation of the lepton number exists so far.

If one assumes that there exist, in addition to the left-handed neutrino fields $\nu_{\ell L}$, right-handed neutrino fields $\nu_{\ell R}$, the neutrino mass Lagrangian may contain also the Dirac mass terms $-M^D_{\ell\ell'} \overline{\nu_{\ell R}} \nu'_\ell$ + h.c. and another type of Majorana mass terms $-(1/2) M^R_{\ell\ell'} \overline{(\nu_{\ell R})^C} \nu_{\ell' R}$ + h.c. Unless the Majorana mass terms vanish, the fields ν_i that diagonalize the full mass Lagrangian are two-component Majorana fields obeying the condition ("Majorana condition")

$$\nu_i = \nu_i^C. \tag{5}$$

There are in this case altogether six mass states. It is generally assumed that $M^R_{\ell\ell'} \gg M^D_{\ell\ell'} \gg M^L_{\ell\ell'}$ (the so-called seesaw model [21–25]), implying that three of these six states are light, corresponding to the three ordinary neutrinos appearing in (2), while the other three are very heavy and decouple from the low-energy physics. Even if the mixing between light and heavy sectors is neglected, the relation (2) is still applicable.

A lot of empirical information on the neutrino mixing, that is, the elements of the matrix U, and the neutrino masses has been obtained via solar, atmospheric, reactor, and accelerator neutrino oscillation experiments. The mixing matrix U can be presented in terms of six measurable parameters, three rotation angles and three phases, as follows [26]:

$$U = \begin{pmatrix} c_{12}c_{13} & s_{12}c_{13} & s_{13}e^{-i\delta} \\ -s_{12}c_{23} - c_{12}s_{23}s_{13}e^{i\delta} & c_{12}c_{23} - s_{12}s_{23}s_{13}e^{i\delta} & s_{23}c_{13} \\ s_{12}s_{23} - c_{12}c_{23}s_{13}e^{i\delta} & -c_{12}s_{23} - s_{12}c_{23}s_{13}e^{i\delta} & c_{23}c_{13} \end{pmatrix} P, \tag{6}$$

where $P = \text{diag}(1, e^{i\alpha}, e^{i\beta})$, $s_{ij} = \sin\theta_{ij}$, $c_{ij} = \cos\theta_{ij}$, and δ is called the Dirac phase and α and β the Majorana phases. The probability for the oscillatory transition from the neutrino flavor ν_α to the flavor ν_β as a function of the distance of flight L and neutrino energy E is given by (see, e.g., [27])

$$P\left(\nu_\alpha \longrightarrow \nu_\beta\right) = \delta_{\alpha\beta} - 4\sum_{i>j} \text{Re}\left[U^*_{\alpha i}\ U^*_{\beta j}\ U_{\beta i}\ U_{\alpha j}\right] \sin^2 \frac{\Delta m^2_{ij} L}{4E} + 2\sum_{i>j} \text{Im}\left[U^*_{\alpha i}\ U^*_{\beta j}\ U_{\beta i}\ U_{\alpha j}\right] \sin \frac{\Delta m^2_{ij} L}{2E}, \tag{7}$$

where $\Delta m^2_{ij} = m^2_i - m^2_j$. As can be seen from this formula, the neutrino oscillations do not bring us any information about the absolute neutrino mass scale, only about the squared mass differences Δm^2_{ij}. One can also easily show that neutrino oscillations are not sensitive to the Majorana phases α and β.

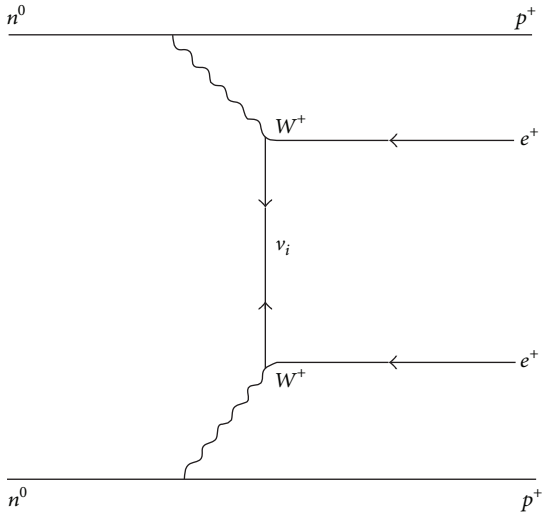

Figure 1: Feynman diagram for the Majorana-neutrino-mediated $\beta^+\beta^+$ decay.

A global fit to oscillation data yields the following values for the parameters [5]:

$$\begin{aligned}
\Delta m^2_{21} &= 7.54^{+0.26}_{-0.22} \times 10^{-5}\text{eV}^2,\\
\Delta m^2_{31} \simeq \Delta m^2_{32} &= 2.43^{+0.06}_{-0.10} \times 10^{-3}\text{eV}^2,\\
\sin^2\theta_{12} &= 0.307^{+0.18}_{-0.16},\\
\sin^2\theta_{23} &= 0.386^{+0.24}_{-0.21},\\
\sin^2\theta_{13} &= 0.0241^{+0.0025}_{-0.0025}.
\end{aligned} \tag{8}$$

Here the normal mass hierarchy $m_3 > m_1, m_2$ is assumed; the values are slightly varied for the inverse hierarchy $m_3 < m_1, m_2$ (see [5]).

The main goals of the forthcoming neutrino oscillation experiments are to measure the value of the CP phase δ and to determine the neutrino mass hierarchy, whether it is normal or inverted. The other important open questions of neutrino physics include determining the absolute mass scale of neutrinos and finding out whether neutrinos are Dirac particles or Majorana particles. These latter two questions could be at least partially solved by neutrinoless double beta decay and other lepton number violating processes. Information about the absolute neutrino mass can be also obtained by determining the effective electron neutrino mass $m_\beta = \sqrt{\sum_i |U_{ei}|^2 m_i^2}$ in beta decay experiments, as well as from the cosmological precision measurements of the sum of neutrino masses $\sum_i m_i$. The current experimental upper limits for m_β are 2.3 eV [28] and 2.1 eV [29], and for the sum of neutrino masses $\sum_i m_i$ the recent Planck satellite data [6] imply the upper limit 0.66 eV.

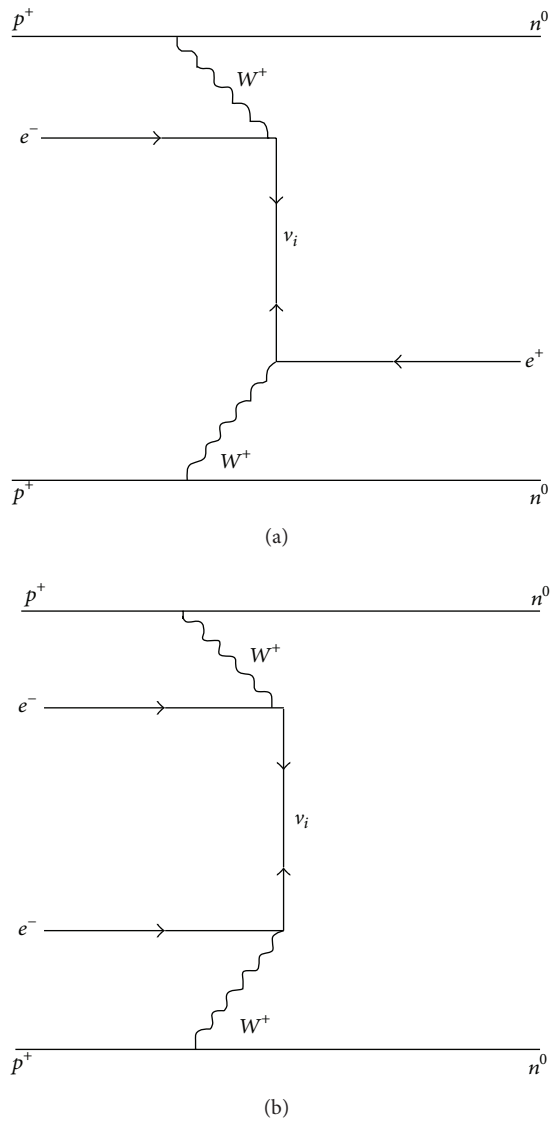

Figure 2: Feynman diagrams for the Majorana-neutrino-mediated β^+EC (a) and ECEC (b) decays.

3. Neutrino Masses and Double Beta Decay

In the standard picture the neutrinoless double beta decays $(A, Z) \rightarrow (A, Z+2) + 2e^-$ and $(A, Z) \rightarrow (A, Z-2) + 2e^+$ are mediated by light neutrinos. These processes are of great importance from the particle-physics point of view, as they would indicate the violation of lepton number, which in turn would imply that light neutrinos are Majorana particles. This would be valuable information for understanding the origin of fermion masses.

We are considering in this work particularly the positron-emission mode $(A, Z) \rightarrow (A, Z-2) + 2e^+$ (see Figure 1). In the electroweak model the leptonic part of this process is described by a second-order perturbation given by

$$\left(\frac{G_F}{\sqrt{2}}\right)^2 \overline{e^+}\gamma_{\mu'}\left(1+\gamma_5\right)\nu_e^c\overline{\nu_e}\gamma_\mu\left(1-\gamma_5\right)e^-, \tag{9}$$

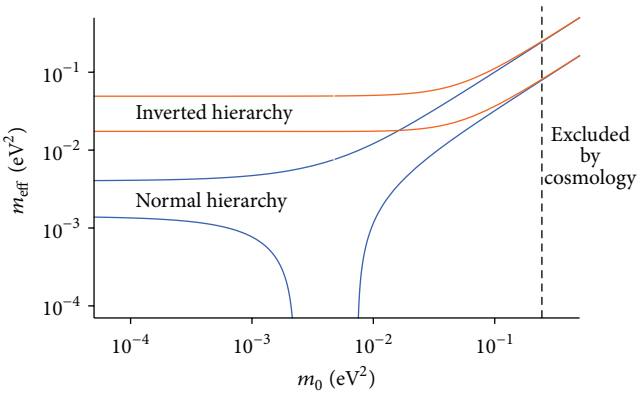

FIGURE 3: Absolute value of the effective neutrino mass $m_{\text{eff}} = |\langle m_\nu \rangle|$ against the mass m_0 of the lightest neutrino for both the normal and inverted mass hierarchy and for all possible values of the phases φ_{12} and φ_{13} defined in (15). The best-fit values [5] are used for the oscillation parameters (see (8)). The cosmological upper limit for m_0, derived from the Planck satellite measurements [6], is also given.

where e^-, e^+, ν_e, and ν_e^c are the field operators of the electron, positron, electron neutrino, and electron antineutrino, respectively. The strength of the interaction is governed by the Fermi coupling constant $G_F/\sqrt{2} = g^2/(8m_W^2)$, where g is the fundamental gauge coupling of the electroweak theory and m_W is the mass of $W^\pm$. The propagator describing the internal neutrino is given by

$$\begin{aligned}
&\langle 0 \left| \nu_e^c(x)\, \bar{\nu}_e(y) \right| 0 \rangle \\
&\quad = \sum_i (U_{ei}^*)^2 \langle 0 \left| \nu_i(x)\, \bar{\nu}_i(y) \right| 0 \rangle \\
&\quad = -i \sum_i (U_{ei}^*)^2 \int \frac{d^4q}{(2\pi)^4} \frac{\not{q} + m_i}{q^2 - m_i^2} \exp\left(-iq \cdot (x-y)\right),
\end{aligned} \tag{10}$$

where the condition (5) is used.

The amplitude of the process $(A, Z) \to (A, Z-2)+2e^+$ is proportional to

$$\sum_i G_F^2 U_{ei}^{*2} \gamma_\mu \gamma_L \frac{\not{q} + m_i}{q^2 - m_i^2} \gamma_{\mu'} \gamma_L = \sum_i G_F^2 U_{ei}^{*2} \frac{m_i}{q^2 - m_i^2} \gamma_\mu \gamma_R \gamma_{\mu'}, \tag{11}$$

where q is the momentum of the exchanged neutrino and $\gamma_{L(R)}$ are the chirality projection matrices $\gamma_{L(R)} = (1(-/(+))\, \gamma_5)/2$. Note that the $\not{q}$ part of the neutrino propagator does not contribute due to chirality mismatch. Typically $q \simeq 100$ MeV, in accordance with a typical nuclear distance of 1 fm. Given that neutrinos are expected to be in the sub-eV mass scale, one can safely approximate the denominator of the neutrino propagator by q^2, leading to

$$G_F^2 \left(\sum_i U_{ei}^{*2} m_i \right) \frac{1}{q^2} \gamma_\mu \gamma_R \gamma_{\mu'}. \tag{12}$$

The essential part of the amplitude from neutrino-physics point of view is the quantity:

$$\langle m_\nu \rangle \equiv \sum_i U_{ei}^{*2} m_i, \tag{13}$$

whose absolute value is called the effective neutrino mass; that is,

$$m_{\text{eff}} = \left| \langle m_\nu \rangle \right|. \tag{14}$$

Although this quantity depends on a great number of observables, it is associated with just one single parameter of the fundamental Lagrangian, the Majorana mass term of the left-handed electron neutrino M_{ee}^L (see (3)).

The modes β^+EC and ECEC (Figure 2) are described by the same operator (9) as the $\beta^+\beta^+$ mode, which is easily understandable since the antiparticle creation operator is always associated with the particle annihilation operator in the fermion fields. Hence all these processes probe the same effective neutrino mass. The decay rates of the processes are proportional to $|\langle m_\nu \rangle|^2$.

Using the standard parametrization (6) of the mixing matrix U, one can cast $\langle m_\nu \rangle$ in the following form:

$$\langle m_\nu \rangle = c_{12}^2 c_{13}^2 m_1 + s_{12}^2 c_{13}^2 e^{-i\varphi_{12}} m_2 + s_{13}^2 e^{-i\varphi_{13}} m_3, \tag{15}$$

where $\varphi_{12} = \alpha$ and $\varphi_{13} = \beta - \delta$. Depending on the phases φ_{12} and φ_{13}, the contributions of the three neutrino mass states will add up constructively or destructively. In the case the CP symmetry is conserved, the phase factors assume the values +1 or −1, depending on the intrinsic CP quantum numbers of the mass states, which in turn depend on the detailed structure of the mass matrix. There are four possible sign combinations which lead to different values for $\langle m_\nu \rangle$. Any values of the phases different from ±1 would mean violation of the CP symmetry.

The amplitude of the electron-electron decay mode is proportional to the complex conjugate of $\langle m_\nu \rangle$. As the decay widths are proportional to $|\langle m_\nu \rangle|^2$, the modes $\beta^+\beta^+$ and $\beta^-\beta^-$, as well as of the modes β^+EC and ECEC, probe neutrino physics through the same quantity. Hence the CP is not manifestly broken in neutrinoless double beta decay, although the Majorana phases φ_{12} and φ_{13} appear in $\langle m_\nu \rangle$. One can understand this also as a consequence of the fact that in the limit $q^2 \gg m_i^2$ the amplitudes depend on just one parameter of the mass Lagrangian, the element M_{ee}^L, allowing for no measurable phases. To be sensitive to the Majorana CP phases, one should be able to distinguish between the mass states ν_i.

Apart from the CP phases φ_{12} and φ_{13}, which are not observables of neutrino oscillations (the possible CP violation in oscillation phenomena is due to the Dirac phase δ), there are two unknowns in the expression of the effective mass, namely, the absolute neutrino mass scale, say the mass m_0 of the lightest neutrino, and the mass hierarchy, that is, whether $m_3 > m_1, m_2$ (normal hierarchy) or $m_3 < m_1, m_2$ (inverted hierarchy). All three neutrino masses can be

expressed in terms of the absolute mass m_0: in the case of the normal hierarchy

$$m_1 = m_0,$$
$$m_2 = \sqrt{m_0^2 + \Delta m_{21}^2}, \quad (16)$$
$$m_3 = \sqrt{m_0^2 + \Delta m_{31}^2},$$

and in the case of inverted hierarchy

$$m_1 = \sqrt{m_0^2 + |\Delta m_{31}^2|},$$
$$m_2 = \sqrt{m_0^2 + \Delta m_{21}^2 + |\Delta m_{31}^2|}, \quad (17)$$
$$m_3 = m_0.$$

The squared mass difference Δm_{21}^2 and the absolute value of the mass difference Δm_{31}^2 are known from neutrino oscillation experiments. The neutrino hierarchy will be determined in the forthcoming neutrino oscillation experiments. This information would be crucial for interpretation of the results of the double beta decay experiments. In the case of inverted hierarchy, $|\langle m_\nu \rangle|$ has lower limit of the order of 10^{-2} eV, as can be inferred from Figure 3, where the effective mass, $m_{\text{eff}} = |\langle m_\nu \rangle|$, is presented as a function of the mass m_0 of the lightest neutrino for all possible values of the Majorana phases φ_{12} and φ_{13}. If no signal of double beta decay is obtained above this limit, it would mean that either the hierarchy has to be the normal one or the neutrino is not a Majorana particle. An observation of double beta transition with $|\langle m_\nu \rangle| < 10^{-2}$ eV would mean that the mass hierarchy is normal and the neutrino is a Majorana particle. On the other hand, nonobservation of the transition would not mean that the process does not exist, since in the case of the normal mass hierarchy the effective mass and hence the decay width can be arbitrarily small.

4. Double Beta Decays on the β^+/ Electron-Capture Side

In this section a rather detailed account of the basic theoretical ingredients of the half-life calculations is given. In this way the reader can have a unified picture of the formalisms used for various types of double beta transitions.

4.1. Half-Lives and Nuclear Matrix Elements. In this work it is assumed that the $0\nu\beta^+$/EC decays proceed exclusively via the exchange of massive Majorana neutrinos, as discussed in Section 3. The inverse half-lives for the neutrinoless $\beta^+\beta^+$ and β^+EC decays can be cast in the form

$$\left[T_{0\nu}^{\alpha}(0^+)\right]^{-1} = G_{0\nu}^{\alpha}(0^+)\left|M^{(0\nu)\prime}\right|^2 (m_{\text{eff}}\,[\text{eV}])^2, \quad (18)$$
$$\alpha = \beta^+\beta^+,\ \beta^+\text{EC},$$

where m_{eff} is the effective neutrino mass (14) that should be given in (18) in units of eV. The decays described by (18) proceed via the available phase space for the final state leptons and the phase-space integrals $G_{0\nu}^{\beta^+\beta^+}(0^+)$ and $G_{0\nu}^{\beta^+\text{EC}}(0^+)$ are defined in [7]. The involved nuclear matrix element (NME) can be written (see, e.g., [45–47]) in terms of the Gamow-Teller (GT), Fermi (F), and tensor (T) matrix elements in the form

$$M^{(0\nu)\prime} = \left(\frac{g_A}{1.25}\right)^2 \left[M_{\text{GT}}^{(0\nu)} - \left(\frac{g_V}{g_A}\right)^2 M_{\text{F}}^{(0\nu)} + M_{\text{T}}^{(0\nu)}\right], \quad (19)$$

where $g_A = 1.25$ corresponds to the bare-nucleon value of the axial-vector coupling constant and $g_V = 1.00$ is the vector coupling constant. The tensor matrix element is neglected in the present calculations since its contribution is very small [48, 49]. The above defined NME is convenient since the phase-space factor to be used with it is always the one defined for $g_A = 1.25$ independent of the value of g_A used in (19).

In the case of the neutrinoless double electron capture, 0νECEC, there are no leptons available in the final state to carry away the decay energy. In this case one has to engage some additional mechanism to rid the initial atom of the excess energy of decay. There are two proposed mechanisms to cope with this situation: the radiative 0νECEC decay [9] and the resonant decay, R0νECEC [8]. The resonance condition—close degeneracy of the initial and final (excited) atomic states—can enhance the decay rate by a factor as large as 10^6. The R0νECEC process is of the form

$$e^- + e^- + (A, Z) \longrightarrow (A, Z-2)^* \longrightarrow (A, Z-2) + \gamma + 2X, \quad (20)$$

where the capture of two atomic electrons leaves the final atom in an excited state, in most cases having the final nucleus in an excited state. The excited state of the nucleus decays by one or more gamma rays and the atomic vacancies is filled by outer electrons with emission of X-rays.

Fulfillment of the resonance condition depends on the so-called degeneracy parameter $Q-E$, where E is the excitation energy of the final atomic state and Q is the difference between the initial and final atomic masses. Possible candidates for such resonant decays are many and a representative list will be displayed in Section 7. The final nuclear states with spin-parity 0^+ are the most favorable ones and the only ones discussed as examples in this review. The inverse half-life for transitions to 0^+ states can be written as

$$\left[T_{0\nu}^{\text{ECEC}}(0^+)\right]^{-1} = g_{0\nu}^{\text{ECEC}}(0^+)\left|M^{(0\nu)\prime}\right|^2 \frac{m_{\text{eff}}^2 \Gamma}{(Q-E)^2 + \Gamma^2/4}, \quad (21)$$

where the daughter state $(A, Z-2)^*$ is a virtual state with energy

$$E = E^* + E_H + E_{H'} + E_{HH'}, \quad (22)$$

including the possible nuclear excitation energy and the binding energies of the two captured electrons. The last term accounts for the Coulomb repulsion between the two holes.

The quantity Γ denotes the combined nuclear and atomic radiative widths where the atomic widths dominate and are a few tens of electron volts [50]. The factor $g_{0\nu}^{\mathrm{ECEC}}$ can be called the atomic factor and it contains the information about the density distributions of the involved atomic orbitals at the nucleus. It can be written as

$$g_{0\nu}^{\mathrm{ECEC}}\left(0^{+}\right)=\left(\frac{G_{\mathrm{F}}\cos\theta_{C}}{\sqrt{2}}\right)^{4}\frac{g_{A}^{4}}{4\pi^{2}\ln 2R_{A}^{2}}m_{e}^{6}\mathcal{N}_{n,\kappa}\mathcal{N}_{n',\kappa'}, \tag{23}$$

where $\mathcal{N}_{n,\kappa}$ is the normalization of the relativistic Dirac wave function for the atomic orbital specified by the quantum numbers (n,κ) [7] in the presence of a uniformly charged spherical nucleus.

The Gamow-Teller and Fermi NMEs appearing in (19) can be written explicitly in the form

$$\begin{aligned}M_{K}^{(0\nu)}=&\sum_{J^{\pi}}\sum_{J'}\sum_{k_{1}k_{2}}\sum_{pp'nn'}(-1)^{j_{p}+j_{n'}+J+J'}\\&\times\sqrt{2J'+1}\begin{Bmatrix}j_{n}&j_{p}&J\\j_{p'}&j_{n'}&J'\end{Bmatrix}\\&\times m_{K}\left(nn',pp';J';k_{1},k_{2}\right)\\&\times\left(0_{f}^{+}\left\|\left[c_{n'}^{\dagger}\widetilde{c}_{p'}\right]_{J}\right\|J_{k_{1}}^{\pi}\right)\left\langle J_{k_{1}}^{\pi}\mid J_{k_{2}}^{\pi}\right\rangle\left(J_{k_{2}}^{\pi}\left\|\left[c_{n}^{\dagger}\widetilde{c}_{p}\right]_{J}\right\|0_{i}^{+}\right),\end{aligned} \tag{24}$$

where $K=$ F, GT and k_1 and k_2 label the different nuclear-model solutions for a given multipole J^{π}, the set k_1 stemming from the calculation based on the final nucleus and the set k_2 stemming from the calculation based on the initial nucleus. Here the one-body transition densities are $(0_f^+\|[c_{n'}^{\dagger}\widetilde{c}_{p'}]_J\|J_{k_1}^{\pi})$ and $(J_{k_2}^{\pi}\|[c_{n}^{\dagger}\widetilde{c}_{p}]_J\|0_i^+)$, and they are given separately for the different types of 0^+ final states f in Section 4.3.

The two-particle matrix element of (24) can be written as

$$\begin{aligned}&m_{K}\left(nn',pp';J';k_{1},k_{2}\right)\\&=\widehat{J'}\widehat{j_{p}}\widehat{j_{p'}}\widehat{j_{n}}\widehat{j_{n'}}\sum_{\lambda S}(2\lambda+1)(2S+1)F_{K}\\&\quad\times\begin{Bmatrix}l_{p}&l_{p'}&\lambda\\\frac{1}{2}&\frac{1}{2}&S\\j_{p}&j_{p'}&J'\end{Bmatrix}\begin{Bmatrix}l_{n}&l_{n'}&\lambda\\\frac{1}{2}&\frac{1}{2}&S\\j_{n}&j_{n'}&J'\end{Bmatrix}\\&\quad\times\sum_{n_{1}n_{2}lNL}M_{\lambda}\left(n_{1}lNL;n_{n}l_{n}n_{n'}l_{n'}\right)\\&\qquad\times M_{\lambda}\left(n_{2}lNL;n_{p}l_{p}n_{p'}l_{p'}\right)\\&\quad\times\int d^{3}r\phi_{n_{1}l}(\mathbf{r})\,h_{K}\left(r_{12},\frac{1}{2}\left(E_{k_{1}}+E_{k_{2}}\right)\right)\phi_{n_{2}l}(\mathbf{r}),\end{aligned} \tag{25}$$

where $\widehat{j}=\sqrt{2j+1}$ and $r_{12}=|\mathbf{r}_1-\mathbf{r}_2|$ is the relative distance between the two decaying protons. The following auxiliary quantities have been defined

$$F_{\mathrm{F}}=1,\qquad F_{\mathrm{GT}}=6(-1)^{S+1}\begin{Bmatrix}\frac{1}{2}&\frac{1}{2}&S\\\frac{1}{2}&\frac{1}{2}&1\end{Bmatrix}. \tag{26}$$

The quantities M_λ are the Moshinsky brackets that mediate the transformation from the laboratory coordinates $\mathbf{r}_1$ and $\mathbf{r}_2$ to the center-of-mass coordinate $\mathbf{R}=(1/\sqrt{2})(\mathbf{r}_1+\mathbf{r}_2)$ and the relative coordinate $\mathbf{r}=(1/\sqrt{2})(\mathbf{r}_1-\mathbf{r}_2)$. In this way the short-range correlations of the two decaying protons are easily incorporated in the theory. The wave functions $\phi_{nl}(\mathbf{r})$ are taken to be the eigenfunctions of the isotropic harmonic oscillator.

The neutrino potential $h_K(r_{12},E)$, $K=$ F, GT, in the integral of (26) is defined as

$$h_{K}\left(r_{12},E\right)=\frac{2}{\pi}R_{A}\int dq\frac{qh_{K}\left(q^{2}\right)}{q+E-\left(E_{i}+E_{f}\right)/2}j_{0}\left(qr_{12}\right), \tag{27}$$

where j_0 is the spherical Bessel function and the integration is performed over the exchanged momentum q. Here $E_i=M_ic^2$ is the ground-state mass energy of the initial nucleus and E_f the (ground-state or excited-state) mass energy of the final nucleus. In practice the lowest pnQRPA energies of the two sets k_1 and k_2 are normalized such that the energy difference of these energies and the mass energy of the initial nucleus match the corresponding experimental energy difference. The term $h_K(q^2)$ in (27) includes the contributions arising from the short-range correlations, nucleon form factors, and higher-order terms of the nucleonic weak current [51]. For all the $0\nu\beta^+$/EC transitions of this work the NMEs have been computed by the use of both the Jastrow short-range correlations [52] and the UCOM correlations [53, 54]. Both short-range correlators have been recently used in many $0\nu\beta^-\beta^-$ calculations [48, 49, 55–58] and in some $0\nu\beta^+$/EC calculations [36, 59–61].

4.2. Nuclear Models and Model Parameters. In this work the wave functions of the nuclear states involved in the double beta decay transitions are calculated by the use of the quasiparticle random-phase approximation (QRPA) in realistically large single-particle model spaces. The J^{π} states of the intermediate nucleus of the $\beta\beta$ decays are generated by the usual proton-neutron QRPA (pnQRPA) [2, 62] in the form

$$\begin{aligned}\left|\;J_{k}^{\pi}\;\;M\;\right\rangle&=Q^{\dagger}\left(J_{k}^{\pi},M\right)|\mathrm{QRPA}\rangle\\&=\sum_{pn}\left(X_{pn}^{J_{k}^{\pi}}\left[a_{p}^{\dagger}a_{n}^{\dagger}\right]_{JM}-Y_{pn}^{J_{k}^{\pi}}\left[a_{p}^{\dagger}a_{n}^{\dagger}\right]_{JM}^{\dagger}\right)|\mathrm{QRPA}\rangle,\end{aligned} \tag{28}$$

where X and Y are the forward- and backward-going amplitudes of the pnQRPA, obtained by solving the pnQRPA

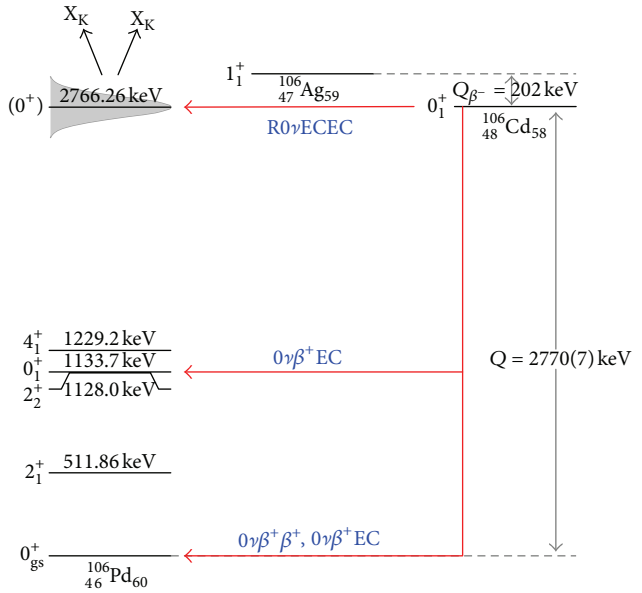

FIGURE 4: Schematic representation of the possible $0\nu\beta^+/\mathrm{EC}$ decay modes of ^{106}Cd. The atomic resonance at 2766.26 keV includes both the nuclear excitation energy and the energy related to the two electron holes in the atomic K shell as given in (22).

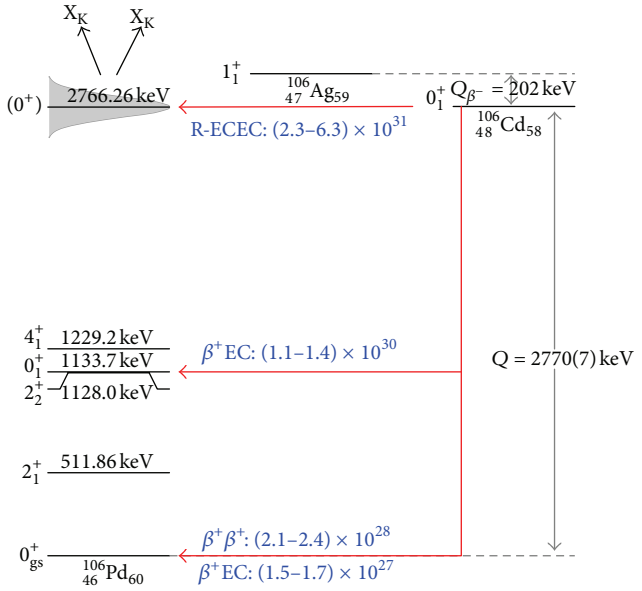

FIGURE 5: Computed partial $0\nu\beta^+/\mathrm{EC}$ decay half-lives of the various decay transitions from ^{106}Cd. The value $m_{\mathrm{eff}} = 0.3$ eV is adopted for the effective neutrino mass and the UCOM short-range correlations have been assumed. The half-lives are given in units of years.

equations of motion [62]. The excited states I_k^π in the final even-even nuclei are described by the phonons of the charge-conserving QRPA (ccQRPA), expressed as

$$\begin{aligned} \left| \; I_k^\pi \;\; M \; \right\rangle &= Q^\dagger \left(I_k^\pi, M\right) |\mathrm{QRPA}\rangle \\ &= \sum_{ab} \left(Z_{ab}^{I_k^\pi} \left[a_a^\dagger a_b^\dagger\right]_{IM} - W_{ab}^{I_k^\pi} \left[a_a^\dagger a_b^\dagger\right]_{IM}^\dagger \right) |\mathrm{QRPA}\rangle \,, \end{aligned} \tag{29}$$

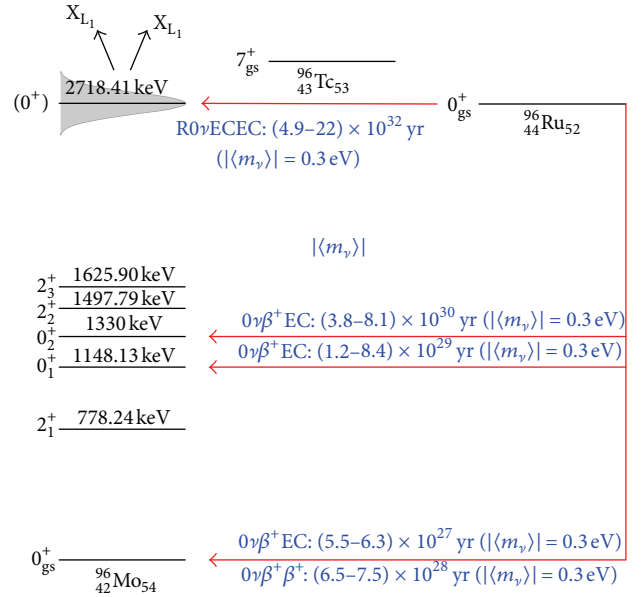

FIGURE 6: Computed partial $0\nu\beta^+/\mathrm{EC}$ decay half-lives of the various decay transitions from ^{96}Ru. The value $m_{\mathrm{eff}} = 0.3$ eV is adopted for the effective neutrino mass and the UCOM short-range correlations have been assumed. The half-lives are given in units of years.

where the symmetrized amplitudes Z and W are obtained from the usual ccQRPA amplitudes X and Y [62] through the transformation

$$Z_{ab}^{I_k^\pi} = \begin{cases} X_{ab}^{I_k^\pi}, & \text{if } a = b \\ \dfrac{1}{2} X_{ab}^{I_k^\pi}, & \text{if } a < b \\ \dfrac{1}{2} X_{ba}^{I_k^\pi}, & \text{if } a > b \end{cases} \tag{30}$$

and similarly for W in terms of Y.

Now one can take a $I_k^\pi = 2_1^+$ phonon of (29) and build an ideal two-phonon I^+ state of the form

$$\left| I_{2-\mathrm{ph}}^+ \right\rangle = \frac{1}{\sqrt{2}} \left[Q^\dagger(2_1^+) Q^\dagger(2_1^+) \right]_I |\mathrm{QRPA}\rangle \,. \tag{31}$$

An ideal two-phonon state consists of partner states $I^\pi = 0^+, 2^+, 4^+$ that are degenerate in energy and exactly at an energy twice the excitation energy of the 2_1^+ state. In practice this degeneracy is always lifted by the residual interaction between the one- and two-phonon states [63]. The one- and two-phonon states in the final even-even nucleus are connected to the J^π states of the intermediate nucleus by transition amplitudes obtained from a higher-QRPA framework called the multiple-commutator model (MCM), first introduced in [64] and further extended in [65].

The calculations were done in sufficiently large single-particle spaces and the single-particle energies were generated by the use of a spherical Coulomb-corrected Woods-Saxon (WS) potential with a standard parametrization [66],

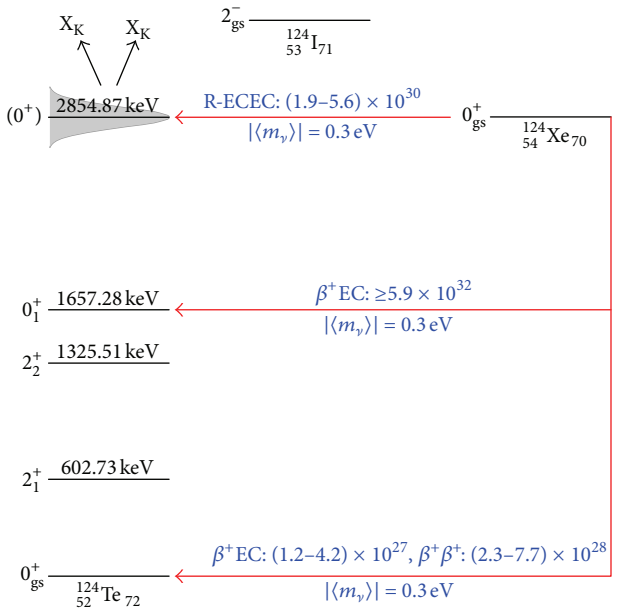

FIGURE 7: Computed partial $0\nu\beta^+$/EC decay half-lives of the various decay transitions from ^{124}Xe. The value $m_{\text{eff}} = 0.3$ eV is adopted for the effective neutrino mass and the UCOM short-range correlations have been assumed. The half-lives are given in units of years.

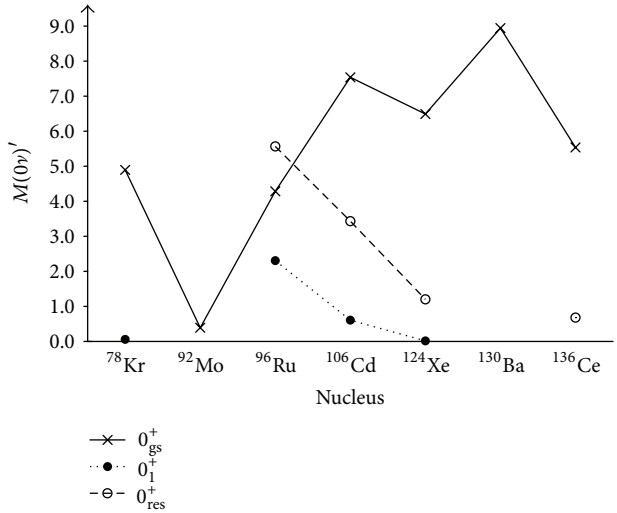

FIGURE 8: Values of the computed nuclear matrix elements for $0\nu\beta^+$/EC decay transitions to the ground state (0^+_{gs}), the first excited 0^+ state (0^+_1) and the resonant 0^+ state (0^+_{res}) for all the nuclei discussed in this paper.

optimized for nuclei near the line of beta stability. Sometimes the Woods-Saxon based single-particle energies were slightly corrected near the proton and/or neutron Fermi surfaces to better reproduce the low-energy spectra of the neighboring neutron-odd and/or proton-odd nuclei at the BCS level. The Bonn-A G-matrix has been used as the two-body interaction and it has been renormalized in the standard way [64, 67]. The quasiparticles are treated in the BCS formalism and the pairing matrix elements are scaled by a common factor,

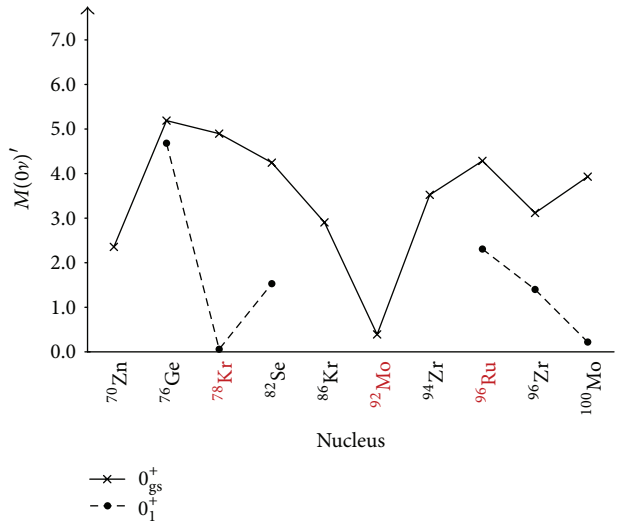

(a)

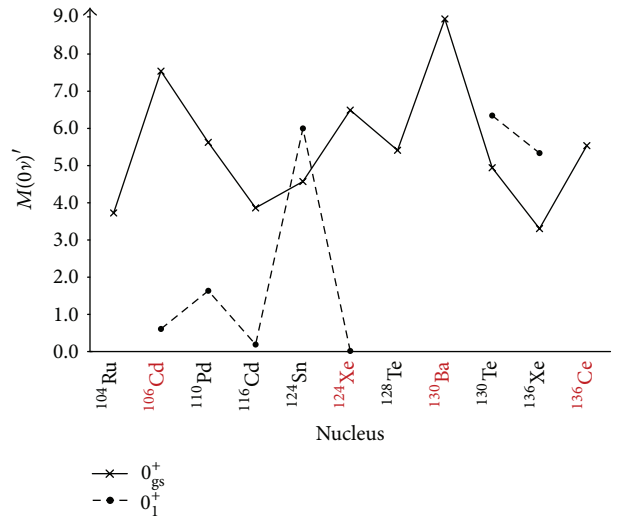

(b)

FIGURE 9: Values of the computed nuclear matrix elements for $0\nu\beta^-\beta^-$ and $0\nu\beta^+$/EC decays for masses $70 \leq A \leq 100$ (a) and for $104 \leq A \leq 136$ (b). Shown are the NMEs corresponding to the decay transitions to the ground state (0^+_{gs}) and the first excited 0^+ state (0^+_1).

separately for protons and neutrons. In practice these factors are fitted such that the lowest quasiparticle energies obtained from the BCS match the experimental pairing gaps for protons and neutrons, respectively [62].

As explained in detail in [45] the particle-hole and particle-particle parts of the proton-neutron two-body interaction are separately scaled by the particle-hole parameter g_{ph} and particle-particle parameter g_{pp}. The value of the particle-hole parameter was fixed by the available systematics [62] on the location of the Gamow-Teller giant resonance (GTGR) state. The value of the g_{pp} parameter regulates the β^--decay amplitude of the first 1^+ state in the intermediate nucleus [68] and hence also the decay

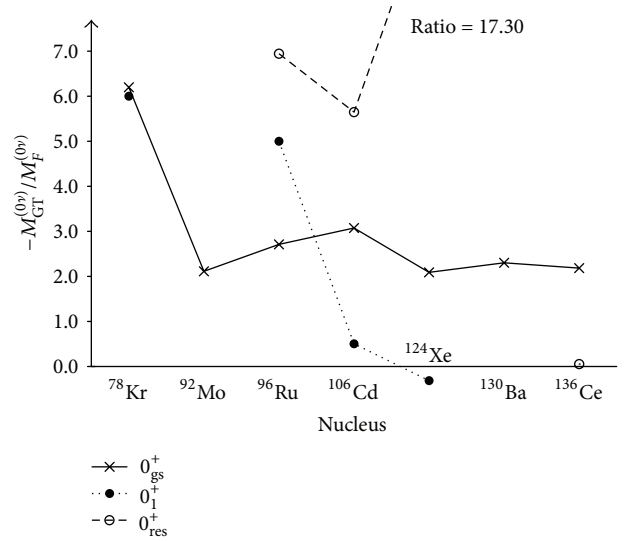

Figure 10: Negative of the ratio between the Gamow-Teller and Fermi NMEs for decays to the ground state (0^+_{gs}), the first excited 0^+ state (0^+_1) and the resonant 0^+ state (0^+_{res}) for all the nuclei discussed in this paper.

rates of the $\beta\beta$ decays. This value can be fixed by either the data on β^- decays [68] or by the data on $2\nu\beta^-\beta^-$-decay rates within the interval $g_A = 1.00$–1.25 of the axial-vector coupling constant [48, 54, 55, 57]. The experimental error and the uncertainty in the value of g_A then induce an interval of physically acceptable values of g_{pp}, the minimum value of g_{pp} related to $g_A = 1.00$ and the maximum value to $g_A = 1.25$. This is because the magnitude of the calculated $2\nu\beta^-\beta^-$ NME, $M^{(2\nu)}$, decreases with increasing value of g_{pp} in a pnQRPA calculation [67, 69, 70] and this magnitude is compared with the magnitude of the experimental NME, $M^{(2\nu)}(\text{exp}) \propto (g_A)^{-2}$, deduced from the experimental $2\nu\beta^-\beta^-$ half-life. The same correspondence between g_{pp} and g_A is adopted also here for the $0\nu\beta^+$/EC decays. In the absence of available half-life data on the $0\nu\beta^+$/EC side the ranges of the adopted g_{pp} values are reasonable choices such that all the physically meaningful values of the $0\nu\beta^+$/EC NMEs are covered.

For the ccQRPA the default value $g_{ph} = 1.0$ was adopted and the g_{pp} parameter was fixed such that the experimental energy of the first 2^+ state in the reference even-even nucleus was reproduced in the ccQRPA calculation.

4.3. Transition Densities. The various transition densities involved in the decay amplitudes (24) are addressed in this section. The initial-branch transition density remains always the same, namely,

$$\left(J^\pi_{k_2}\left\|\left[c^\dagger_n\widetilde{c}_p\right]_J\right\|0^+_i\right) = \widehat{J}(-1)^{j_p+j_n+J+1}\left[v_p u_n X^{J^\pi_{k_2}}_{pn} + u_p v_n Y^{J^\pi_{k_2}}_{pn}\right]. \tag{32}$$

The transition density corresponding to the final ground state reads

$$\left(0^+_{gs}\left\|\left[c^\dagger_{n'}\widetilde{c}_{p'}\right]_J\right\|J^\pi_{k_1}\right) = \widehat{J}(-1)^{j_{p'}+j_{n'}+J+1}\left[\overline{u}_{p'}\overline{v}_{n'}\overline{X}^{J^\pi_{k_1}}_{p'n'} + \overline{v}_{p'}\overline{u}_{n'}\overline{Y}^{J^\pi_{k_1}}_{p'n'}\right], \tag{33}$$

where v ($\overline{v}$) and u ($\overline{u}$) correspond to the BCS occupation and unoccupation amplitudes of the initial (final) even-even nucleus. The amplitudes X and Y ($\overline{X}$ and $\overline{Y}$) come from the pnQRPA calculation starting from the initial (final) nucleus of the $0\nu\beta^+$/EC decay.

For the excited states the multiple-commutator model (MCM) [64, 65] is used. It is designed to connect excited states of an even-even reference nucleus to states of the neighboring odd-odd nucleus. The states of the odd-odd nucleus are given by the pnQRPA and the excited states of the even-even nucleus are generated by the ccQRPA [71]. The ccQRPA phonon (29) defines a state in the final nucleus of the double beta decay. In particular, if this final state is the kth I^+ state, the related transition density, to be inserted in (24), becomes

$$\begin{aligned}\left(I^+_k\left\|\left[c^\dagger_{n'}\widetilde{c}_{p'}\right]_L\right\|J^\pi_{k_1}\right) &= 2\widehat{I}\widehat{L}\widehat{J}(-1)^{L+I+J}\\ &\times\left(\sum_{p_1}\left[\overline{v}_{p'}\overline{v}_{n'}\overline{X}^{J^\pi_{k_1}}_{p_1n'}\overline{Z}^{I^+_k}_{p'p_1} - \overline{u}_{p'}\overline{u}_{n'}\overline{Y}^{J^\pi_{k_1}}_{p_1n'}\overline{W}^{I^+_k}_{p'p_1}\right]\right.\\ &\quad\times\begin{Bmatrix} J & I & L\\ j_{p'} & j_{n'} & j_{p_1}\end{Bmatrix}\\ &\quad+\sum_{n_1}(-1)^{I+j_{n'}+j_{n_1}}\\ &\quad\quad\times\left[\overline{u}_{p'}\overline{u}_{n'}\overline{X}^{J^\pi_{k_1}}_{p'n_1}\overline{Z}^{I^+_k}_{n'n_1} - \overline{v}_{p'}\overline{v}_{n'}\overline{Y}^{J^\pi_{k_1}}_{p'n_1}\overline{W}^{I^+_k}_{n'n_1}\right]\\ &\quad\left.\times\begin{Bmatrix} J & I & L\\ j_{n'} & j_{p'} & j_{n_1}\end{Bmatrix}\right)\end{aligned} \tag{34}$$

instead of the expression (33) for the ground-state transition. Again v ($\overline{v}$) and u ($\overline{u}$) correspond to the BCS occupation and unoccupation amplitudes of the initial (final) even-even nucleus. The amplitudes X and Y ($\overline{X}$ and $\overline{Y}$) come from the pnQRPA calculation starting from the initial (final) nucleus of the $\beta\beta$ decay. The amplitudes $\overline{Z}$ and $\overline{W}$ are the amplitudes of the kth I^+ state in the final nucleus. In the present applications we discuss only $I^+ = 0^+$ final states.

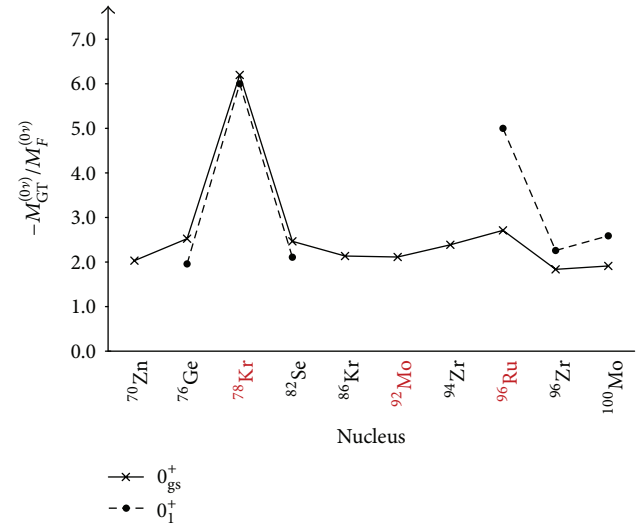

(a)

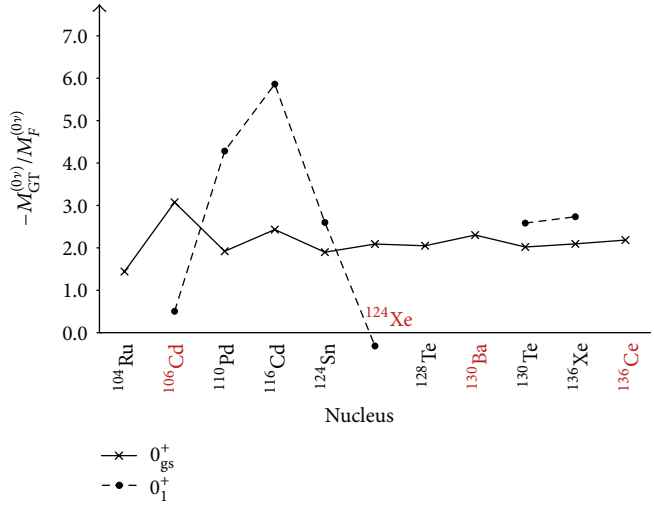

(b)

FIGURE 11: Negative of the ratio between the Gamow-Teller and Fermi NMEs for $0\nu\beta^-\beta^-$ and $0\nu\beta^+$/EC decays for masses $70 \le A \le 100$ (a) and for $104 \le A \le 136$ (b). Shown are the ratios corresponding to the decay transitions to the ground state (0^+_{gs}) and the first excited 0^+ state (0^+_1).

In the case of the two-phonon excitation the transition density to be inserted in (24) attains the form

$$\begin{aligned}
&\left(I^+_{2-\mathrm{ph}} \left\| \left[c^\dagger_{n'}\tilde{c}_{p'}\right]_L \right\| J^\pi_{k_1}\right) \\
&\quad = \frac{40}{\sqrt{2}}\widehat{I}\widehat{L}\widehat{J}(-1)^{I+J+j_{p'}+j_{n'}} \\
&\quad\quad \times \sum_{p_1 n_1} \Big[\overline{v}_{p'}\overline{u}_{n'}\overline{X}^{J^\pi_{k_1}}_{p_1 n_1}\overline{Z}^{2^+_1}_{p' p_1}\overline{Z}^{2^+_1}_{n' n_1} \\
&\quad\quad\quad + \overline{u}_{p'}\overline{v}_{n'}\overline{Y}^{J^\pi_{k_1}}_{p_1 n_1}\overline{W}^{2^+_1}_{p' p_1}\overline{W}^{2^+_1}_{n' n_1} \Big] \\
&\quad\quad \times \begin{Bmatrix} j_{p'} & j_{p_1} & 2 \\ j_{n'} & j_{n_1} & 2 \\ L & J & I \end{Bmatrix},
\end{aligned} \tag{35}$$

where, as usual, the barred quantities denote amplitudes obtained for the final nucleus of double beta decay. In the present work we use only $I^+_{2-\mathrm{ph}} = 0^+$.

5. Typical Examples

In the present paper the neutrinoless $\beta^+\beta^+$ and β^+EC transitions in various nuclei are discussed. Considered are the transitions to the ground state, 0^+_{gs}, and to the first 0^+ state, 0^+_1. The $0\nu\beta^+$/EC decays to only the 0^+ states are considered since large suppression of the mass mode for the decays to 2^+ states is expected [72]. Furthermore, the R0νECEC transitions to the possible resonant states are considered. In the present work the analysis of the R0νECEC half-lives is performed by assuming a 0^+ assignment for the resonant states. This assignment leads to a very likely enhancement in

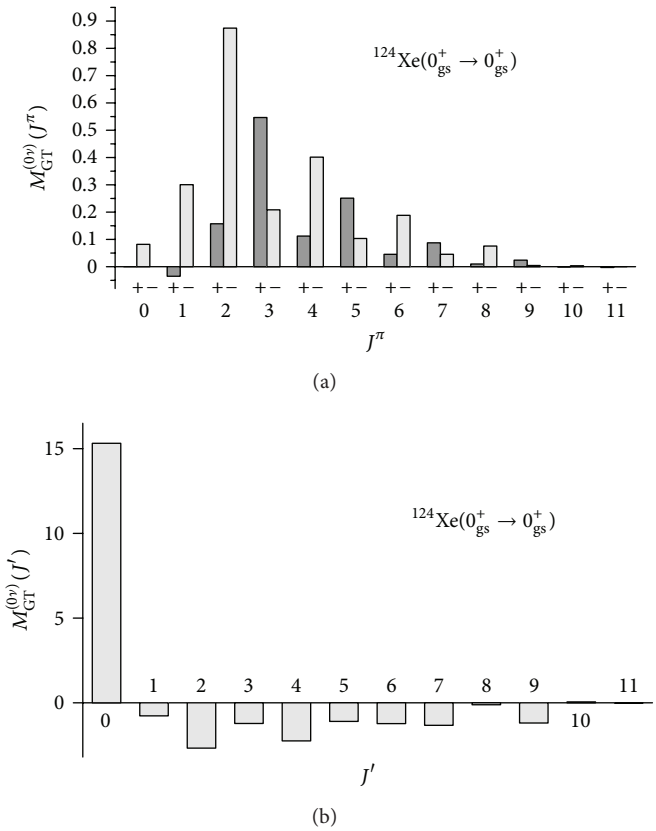

FIGURE 12: Decompositions of (37) in J^π (a) and J' (b) for the ground-state Gamow-Teller NME $M^{(0\nu)}_{GT}(0^+_{gs})$ of ^{124}Xe. Results for the Jastrow short-range correlations are shown with $g_A = 1.25$.

the decay rate. Since this assignment is in many cases only tentative or even unlikely, the calculated half-lives should be taken as optimistic estimates or as lower limits for the half-life.

All the discussed decay transitions are displayed in Figure 4, where the decay of ^{106}Cd serves as paradigm. Both $0\nu\beta^+\beta^+$ and $0\nu\beta^+$EC transitions to the ground state are possible whereas only the $0\nu\beta^+$EC mode is possible for the decay to the 0^+_1 state for phase-space reasons since the $0\nu\beta^+\beta^+$ decay has a negative Q value for this transition. The resonant 0νECEC transition is also shown with the total energy (including the electron-hole contributions, see (22)) of the resonant atomic state.

The various $0\nu\beta^+$/EC decay modes can now be treated by applying the formalisms outlined in Section 4. In particular, the BCS is used to create the quasiparticles in the chosen single-particle valence space and the pnQRPA is used to produce the intermediate J^π states involved in the NME (24). The excited states in the final nucleus are produced by the use of the ccQRPA and the final states are connected to the intermediate J^π states by the MCM prescriptions. After adjusting the parameters of the model Hamiltonian the rates related to the various decay transitions can be evaluated. The results are shown in our paradigm case in Figure 5 for the range $g_A = 1.00$–1.25 of the axial-vector coupling constant and for the value $m_{\text{eff}} = 0.3$ eVof the effective neutrino mass (14).

As seen from Figure 5, the fastest decay mode is $0\nu\beta^+$EC to the ground state of ^{106}Pd with a half-life of $(1.5$–$1.7) \times 10^{27}$ years. This could be in the range of detection sensitivity of the next generation of double beta experiments. The resonance transition proceeds by the capture of two K electrons and emission of two K X-rays, has a half-life of $(2.3$–$6.3) \times 10^{31}$ years, and is thus very hard to be detected in the foreseeable future.

In Figure 6 the half-lives of decay transitions in ^{96}Ru are shown for the range $g_A = 1.00$–1.25 and for the value $m_{\text{eff}} = 0.3$ eV. Again the fastest transition is $0\nu\beta^+$EC to the ground state of ^{96}Mo with a half-life of $(5.5$–$6.3) \times 10^{27}$ years, slightly slower than in the case of ^{106}Cd decay. Interestingly enough there are decays to two excited 0^+ states at energies 1148.13 keVand 1330 keV. The latter state is assumed to be a two-phonon state discussed in this paper, the former one being a one-ccQRPA-phonon state. In this case the resonant decay proceeds with the capture of two L_1 electrons and emission of two L_1 X-rays. The computed half-life for the resonant decay is $(4.9$–$22) \times 10^{32}$ years which is impossible to be detected in the foreseeable future.

The last example of this section pertains to the $0\nu\beta^+$/EC decays in ^{124}Xe, shown in Figure 7. The ranges $g_A = 1.00$ – 1.25 and $m_{\text{eff}} = 0.3$ eV were adopted in the calculations. The $0\nu\beta^+$EC decay to the ground state of ^{124}Te is the fastest with a half-life of $(1.2$–$4.2) \times 10^{27}$ years, being in the range of

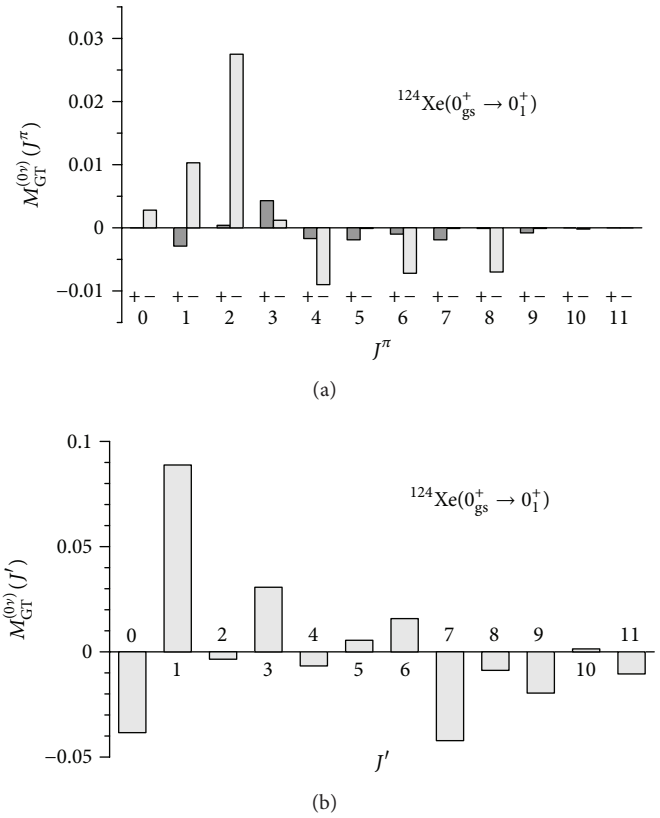

Figure 13: The same as in Figure 12 for the two-phonon NME $M_{GT}^{(0\nu)}(0_1^+)$ corresponding to the 0_1^+ state at 1657 keV in ^{124}Te.

the corresponding decay transition in ^{106}Cd. The decay to the resonance state at 2854.87 keV proceeds with the capture of two K electrons and emission of two K X-rays. The computed half-life is $(1.9–5.6) \times 10^{30}$ years and is thus the fastest of the three discussed example cases, though hard to be detected in the near future.

The computed half-lives can be expressed by the use of the auxiliary quantities $C^{\beta^+\beta^+}$ and $C^{\beta^+\mathrm{EC}}$ in the following form:

$$T_{1/2}^{\beta^+\beta^+} = C^{\beta^+\beta^+}\left(m_{\mathrm{eff}}\,[\mathrm{eV}]\right)^{-2},$$
$$T_{1/2}^{\beta^+\mathrm{EC}} = C^{\beta^+\mathrm{EC}}\left(m_{\mathrm{eff}}\,[\mathrm{eV}]\right)^{-2}, \quad (36)$$

where the effective neutrino mass should be inserted in units of eV. In Table 1 the auxiliary factors of the above equations are given for the nuclei and transitions under discussion. The UCOM short-range correlations have been used combining the results for the possible different basis sets used in the nuclear structure calculations and for the range $g_A = 1.00–1.25$ of the axial-vector coupling constant.

From Table 1 it can be evidenced that generally the fastest transitions are the $0\nu\beta^+$EC transitions to the ground state and transitions to the excited 0^+ state(s) are quite much suppressed relative to the ground-state transitions.

6. Systematic Features of the Nuclear Matrix Elements

There are not too many nuclei that have reasonable Q values and decay by $0\nu\beta^+$/EC decays, and only part of these can have a reasonable chance of decaying via the resonant neutrinoless double EC channel. It is nevertheless instructive to have a fresh view at the systematic features of the involved NMEs.

6.1. The $0\nu\beta^+$/EC NMEs. A systematics of the computed NMEs of the $0\nu\beta^+$/EC decays is shown in Figure 8. The values of NMEs for decays to the ground state (0^+_{gs}), first excited 0^+ state (0^+_1) and the resonant 0^+ state (0^+_{res}) are shown. As mentioned before the assignment of $J^\pi = 0^+$ to the resonant states has to be taken in some cases, like for the ^{106}Cd decay, with a grain of salt. From the figure one notices that the ground-state NMEs are rather large (5.0 or more), except for ^{92}Mo. This means that matrix-element-wise the $0\nu\beta^+$/EC decays are not suppressed relative to the $0\nu\beta^-\beta^-$ decays. This can be further evidenced in Figure 9 where these NMEs are shown together with those of $0\nu\beta^-\beta^-$ decays for nuclei with $70 \le A \le 100$ (a) and for nuclei with $104 \le A \le 136$ (b).

In Figure 8 it is seen that the NMEs corresponding to the resonant 0^+ states are larger than the NMEs corresponding to the decays to 0^+_1 states. This stems from the fact that the resonant states are treated as one-ccQRPA-phonon states

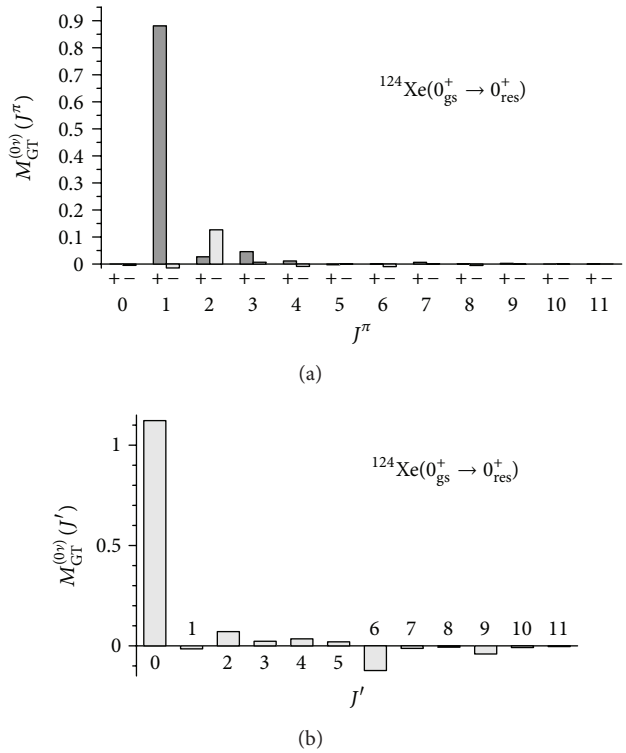

FIGURE 14: The same as in Figure 12 for the resonance NME $M_{GT}^{(0\nu)}(0^+_{res})$ corresponding to the 0^+ state at 2790 keV of nuclear excitation in ^{124}Te.

TABLE 1: Auxiliary factors of (36) computed for the nuclei under discussion by using $g_A = 1.00$–1.25 and the UCOM short-range correlations. The results for ^{92}Mo and ^{136}Ce are taken from [30] with $g_A = 1.261$.

Nucleus	State	$C^{\beta^+\beta^+}$	$C^{\beta^+\mathrm{EC}}$
^{78}Kr	0^+_{gs}	$(9.4–16) \times 10^{26}$	$(3.9–6.5) \times 10^{26}$
	0^+_1	—	$(1.7–4.8) \times 10^{31}$
^{92}Mo	0^+_{gs}	—	6.7×10^{29}
^{96}Ru	0^+_{gs}	$(5.9–6.7) \times 10^{27}$	$(5.0–5.7) \times 10^{26}$
	0^+_1	—	$(1.0–7.6) \times 10^{28}$
	0^+_2	—	$(3.4–7.3) \times 10^{29}$
^{106}Cd	0^+_{gs}	$(1.9–2.2) \times 10^{27}$	$(1.3–1.5) \times 10^{26}$
	0^+_1	—	$(9.8–12.2) \times 10^{28}$
^{124}Xe	0^+_{gs}	$(2.1–6.9) \times 10^{27}$	$(1.1–3.7) \times 10^{26}$
	0^+_1	—	$>5.3 \times 10^{31}$
^{130}Ba	0^+_{gs}	$(5.3–15.9) \times 10^{27}$	$(5.6–16.9) \times 10^{25}$
	0^+_1	—	—
^{136}Ce	0^+_{gs}	2.7×10^{29}	4.0×10^{26}

whereas the 0^+_1 states are described as two-ccQRPA-phonon states. The MCM connects the two-phonon states weaker than the one-phonon states to the J^π states of the neighboring odd-odd nucleus due to the ZZ products and the $9j$ symbol appearing in the associated transition density (35).

From Figure 9 it is seen that the $0\nu\beta^+$/EC NMEs show local maxima (^{96}Ru, ^{106}Cd, ^{124}Xe, ^{130}Ba, and ^{136}Ce) for the ground-state transitions and even a global maximum: ^{130}Ba. On the other hand, ^{92}Mo shows a global minimum. For the decays to the 0^+_1 states the $0\nu\beta^+$/EC NMEs are small relative to the $0\nu\beta^-\beta^-$ NMEs, except for ^{96}Ru which has a relatively large NME.

6.2. Fermi and Gamow-Teller Parts of the $0\nu\beta^+$/EC NMEs. One can also scrutinize the decomposition of the $0\nu\beta^+$/EC NMEs to their Fermi and Gamow-Teller constituents. This decomposition is shown in Figure 10 where the negative of the ratio of these two constituents has been plotted for decays to the different final states, 0^+_{gs}, 0^+_1, and 0^+_{res}. In Figure 11 the same has been done in a global context by including also the ratios for the $0\nu\beta^-\beta^-$ emitters. In this figure one notices that the ratios have a rather universal value of roughly 2.0, except in the case of ^{78}Kr that has a ratio of about 6.0. The ratios for the 0^+_1 transitions show pronounced peaks for the $0\nu\beta^+$/EC emitters ^{78}Kr and ^{96}Ru and for the $0\nu\beta^-\beta^-$ emitters ^{110}Pd and ^{116}Cd, whereas pronounced minima occur for ^{106}Cd and ^{124}Xe. Mostly these ratios for the 0^+_1 are slightly above 2.0.

All in all, much more variation in the Gamow-Teller/Fermi ratio is seen for the 0^+_1 states than for the ground states. From Figure 10 it is clear that the ratios for the resonant states are much higher than for the 0^+_1 or 0^+_{gs} states in the corresponding nuclei.

6.3. Decompositions of the $0\nu\beta^+$/EC NMEs. The $0\nu\beta^+$/EC NMEs can be decomposed into contributions of different intermediate multipoles as done in [59] for ^{96}Ru. Let us use here the decay of ^{124}Xe as an example. The decomposition of the $0\nu\beta$/EC NMEs $M^{(0\nu)'}$ (19) can be made in two ways, either through the different multipole states J^π of the intermediate nucleus (in this case the states of ^{124}I) or through different couplings J' of the two decaying nucleons [57, 73]. For the Gamow-Teller NME these decompositions can be schematically written as

$$M_{GT}^{(0\nu)} = \sum_{J^\pi} \sum_{J'} M_{GT}^{(0\nu)}\left(J^\pi, J'\right), \tag{37}$$

where $M_{GT}^{(0\nu)}(J^\pi, J')$ is given explicitly in (24). The decompositions (37) are shown for the Gamow-Teller NMEs of the decays of ^{124}Xe in Figures 12, 13, and 14. All the figures refer to calculations using the Jastrow short-range correlations and the value $g_A = 1.25$ for the axial-vector coupling constant.

From the decomposition figures one can make the following general observations. For the ground-state NME the decomposition in terms of J^π is the typical one of the pnQRPA calculations [45, 57, 59] and the decomposition in terms of J' is typical of the shell-model [73] and pnQRPA [36, 57, 59] calculations. Here typical for the J^π decomposition are the strong contributions of the high-multipole components $2^-, 3^+, 4^-$, and 5^+. In this case the 1^+ contribution is modest contrary to that of the ^{96}Ru

Table 2: Comparison of the ground-state NMEs for the QRPA, IBM-2 [31], and PHFB [32] models using the Jastrow short-range correlations. The results for ^{136}Ce are taken from [30] with $g_A = 1.261$.

Nucleus	QRPA ($g_A = 1.25$)			IBM-2 ($g_A = 1.269$)			PHFB ($g_A = 1.254$)
	$M_{\mathrm{GT}}^{(0\nu)}$	$M_{\mathrm{F}}^{(0\nu)}$	$M^{(0\nu)\prime}$	$M_{\mathrm{GT}}^{(0\nu)}$	$M_{\mathrm{F}}^{(0\nu)}$	$M^{(0\nu)\prime}$	$M^{(0\nu)\prime}$
^{78}Kr	3.271	−0.331	3.482	3.384	−2.146	4.478	—
^{96}Ru	2.589	−0.988	3.222	2.204	−0.269	2.483	4.82 ± 0.11
^{106}Cd	4.920	−1.586	5.935	2.757	−0.255	3.106	7.97 ± 0.72
^{124}Xe	3.491	−1.889	4.700	3.967	−2.224	5.156	3.69 ± 0.32
^{130}Ba	5.412	−2.528	7.031	3.911	−2.108	5.043	2.75 ± 0.82
^{136}Ce	4.282	−1.961	5.537	3.815	−2.007	4.901	—

Table 3: Comparison of the 0_1^+ NMEs for the QRPA and IBM-2 [31] models using the Jastrow short-range correlations.

Nucleus	QRPA ($g_A = 1.25$)			IBM-2 ($g_A = 1.269$)		
	$M_{\mathrm{GT}}^{(0\nu)}$	$M_{\mathrm{F}}^{(0\nu)}$	$M^{(0\nu)\prime}$	$M_{\mathrm{GT}}^{(0\nu)}$	$M_{\mathrm{F}}^{(0\nu)}$	$M^{(0\nu)\prime}$
^{78}Kr	0.039	−0.008	0.044	0.771	−0.479	1.014
^{96}Ru	2.004	−0.396	2.258	0.036	−0.012	0.045
^{106}Cd	0.317	−0.537	0.660	1.395	−0.110	1.537
^{124}Xe	−0.005	−0.050	0.028	0.647	−0.359	0.839

decay [59]. This contribution depends strongly on the value of the strength parameter g_{pp}. For the $J^\prime$ decomposition typical is the large positive monopole contribution and the much smaller, mostly negative, and higher-multipole contributions.

For the lowest excited 0^+ state, $0_1^+ = 0_{2-\mathrm{ph}}^+$, the pattern is qualitatively different for the J^π decomposition since the other multipole components than 2^- are suppressed but sizable negative contributions from the higher multipole components appear. The relative contributions of the $1^\pm$ and $2^\pm$ states for the ground-state and 0_1^+ NMEs are surprisingly similar. In the case of the $J^\prime$ decomposition the $J^\prime = 0$ component is not the dominant one but, instead, the $J^\prime = 1$ component is. The higher-multipole components contribute sizably, with varying signs. The multipole decompositions of the 0^+ resonant state, 0_{res}^+, which is a one-phonon ccQRPA state, are rather blunt. They show both a strong $J^\pi = 1^+$ component and a strong monopole $J^\prime = 0$ component. The rest of the contributions play only a minor role.

6.4. Comparison of NMEs Produced by Different Models. In Table 2 we present the results of recent calculations for the NMEs of the discussed nuclei. The QRPA results are the ones of this work, the IBM-2 results are taken from [31], and the projected Hartree-Fock-Bogoliubov (PHFB) results are taken from [32]. The IBA-2 model is based on a phenomenological Hamiltonian with connections to the underlying shell model via a mapping procedure. The PHFB is a mean-field model with phenomenological Hamiltonians. Both IBM-2 and PHFB can explicitly take into account deformation effects whereas the QRPA calculations assume spherical or nearly spherical shapes. Since IBM-2 and PHFB quote their results using the Jastrow short-range correlations, also the QRPA calculations have been done by using these correlations. All the quoted calculations in Table 2 use practically the same value of the axial-vector coupling constant g_A.

From Table 2 one observes that the NMEs computed by the use of the QRPA and IBM-2 are rather similar whereas the PHFB NMEs deviate from them notably. These trends are similar to the ones for the $0\nu\beta^-\beta^-$ decaying nuclei as discussed extensively in [74].

In Table 3 the NMEs corresponding to the $0\nu\beta^+$/EC decays to the first excited 0^+ state, 0_1^+, are shown for the QRPA and the IBM-2. The PHFB model cannot access these NMEs since it is by definition a mean-field model describing only ground-state transitions. What is striking in Table 3 are the very different NMEs and their trends predicted by the two models. The QRPA produces small NMEs for ^{78}Kr, ^{106}Cd, and ^{124}Xe and rather large NME for ^{96}Ru. For IBM-2 the opposite happens. This tension between the two calculations is more drastic than in the case of the $0\nu\beta^-\beta^-$ transitions, as analyzed in [74].

6.5. Experimental Limits for the Half-Lives. Up to now only limits of half-lives have been extracted for the various $0\nu\beta^+$/EC processes. Measurements have been done, for example, for ^{74}Se [75], for ^{96}Ru [76, 77], for ^{106}Cd [78], for ^{112}Sn [79], for ^{136}Ce and ^{138}Ce [80], and for ^{64}Zn and ^{180}W [81]. The obtained lower limits are of the order of 10^{20} years for ^{96}Ru [77] and ^{106}Cd [78] and 10^{15} years for ^{136}Ce [80]. These limits are still very far from the theoretical estimates as implied by Table 1.

7. Present Status of the Resonant Processes

Table 4 lists the known cases of R0νECEC transitions in various nuclei where Q-value measurements have been conducted recently. These Q values have been meas-

Table 4: R0νECEC decay transitions with the final-state spin-parity indicated in the second column and the degeneracy parameters $Q - E$ in the third column. Also the involved atomic orbitals have been given in the fourth column. The second last column lists the currently available half-life estimates with the references to the Q-value measurement and calculations indicated in the last column.

Transition	J_f^π	$Q - E$ [keV]	Orbitals	C^{ECEC}	References
^{74}Se $\rightarrow$ ^{74}Ge	2^+	2.23	L_2L_3	$(0.2–100) \times 10^{43}$	[33]
^{96}Ru $\rightarrow$ ^{96}Mo	2^+	8.92 (13)	L_1L_3		[34]
	0^+?	−3.90 (13)	L_1L_1		
^{102}Pd $\rightarrow$ ^{102}Ru	2^+	75.26 (36)	KL_3		[35]
^{106}Cd $\rightarrow$ ^{106}Pd	0^+?	8.39	KK	$(2.1–5.7) \times 10^{30}$	[36]
	$(2,\ 3)^-$	−0.33 (41)	KL_3		[35]
^{112}Sn $\rightarrow$ ^{112}Cd	0^+	−4.5	KK	$>5.9 \times 10^{29}$	[37]
^{124}Xe $\rightarrow$ ^{124}Te	0^+?	1.86 (15)	KK	$(1.7–5.1) \times 10^{29}$	[38]
^{130}Ba $\rightarrow$ ^{130}Xe	0^+?	10.18 (30)	KK		[38]
^{136}Ce $\rightarrow$ ^{136}Ba	0^+	−11.67	KK	$(3–23) \times 10^{32}$	[39]
^{144}Sm $\rightarrow$ ^{144}Nd	2^+	171.89 (87)	KL_3		[35]
^{152}Gd $\rightarrow$ ^{152}Sm	0^+_{gs}	0.91 (18)	KL_1	$(1.0–1.5) \times 10^{27}$	[40, 41]
^{156}Dy $\rightarrow$ ^{156}Gd	1^-	0.75 (10)	KL_1		[42]
	0^+	0.54 (24)	L_1L_1		[42]
	2^+	0.04 (10)	M_1N_3		[42]
^{162}Er $\rightarrow$ ^{162}Dy	2^+	2.69 (30)	KL_3		[34]
^{164}Er $\rightarrow$ ^{164}Dy	0^+_{gs}	6.81 (13)	L_1L_1	$(3.2–5.2) \times 10^{31}$	[41, 43]
^{168}Yb $\rightarrow$ ^{168}Er	(2^-)	1.52 (25)	M_1M_3		[34]
^{180}W $\rightarrow$ ^{180}Hf	0^+_{gs}	11.24 (27)	KK	$(4.0–9.5) \times 10^{29}$	[41, 44]

ured by using the Penning-trap techniques. In the cases of ^{96}Ru, ^{106}Cd, ^{124}Xe, and ^{130}Ba the assignment of 0^+ spin-parity to the resonant state is uncertain. In these cases further experimental spectroscopy is needed.

In the table we also list the estimated half-lives for the cases for which such exist. The references of the last column indicate the origin of the Q-value measurement and the possible calculations of the related NME. In the table an auxiliary quantity C^{ECEC} is listed and its relation with the R0νECEC half-life stands as

$$T_{1/2}^{\mathrm{R0}\nu\mathrm{ECEC}} = \frac{C^{\mathrm{ECEC}}}{\left(m_{\mathrm{eff}}\,[\mathrm{eV}]\right)^2}\ \text{years}, \tag{38}$$

where the effective neutrino mass should be given in units of eV. In all the listed cases where C^{ECEC} has been computed the decay rates are suppressed by the rather sizable magnitude of the degeneracy parameter. Decays to 0^+ states are favored over the decays to 2^+ or $1^-, 2^-, 3^-$, and so forth states due to the involved nuclear wave functions and/or higher-order transitions. Also captures from atomic orbitals with orbital angular momentum $l > 0$ are suppressed [33].

There are some favorable values of degeneracy parameters listed in Table 4, like ^{106}Cd $\rightarrow$ ^{106}Pd$(2, 3)^-$ and ^{156}Dy $\rightarrow$ ^{156}Gd$(0^+, 1^-, 2^+)$ but the associated nuclear matrix elements are still waiting for their evaluation. Strong suppression of the NMEs related to final states with $J > 0$ is, however, expected. In case of the ^{156}Dy decay the deformation also plays an important role. At the moment the most favorable case with a half-life estimate is the case ^{152}Gd $\rightarrow$ ^{152}Sm(0^+_{gs}) which describes a decay transition to the ground state.

8. Summary and Conclusions

Neutrino masses and their influence on neutrino oscillations and on the nuclear double beta decay have been addressed. The various positron-emitting and/or electron-capture modes of the neutrinoless double beta decays have been investigated for the associated nuclear matrix elements and decay half-lives. A QRPA-based theory framework with G-matrix-based two-body interactions and realistically large single-particle bases has been used in the calculations. The computed values of the nuclear matrix elements have been analyzed and contrasted globally with the double beta minus nuclear matrix elements. Special attention has been paid to the resonant neutrinoless double electron capture process to survey its potential for Majorana-mass detection in dedicated experiments. Generally, the resonance condition is poorly satisfied and the emerging half-lives are extremely hard to measure. Few exceptions occur but the associated nuclear matrix elements are not known. Further theoretical efforts in these cases are stringently called for.

Acknowledgment

This work was partly (Jouni Suhonen) supported by the Academy of Finland under the Finnish Center of Excellence Program 2012–2017 (Nuclear and Accelerator Based Program at JYFL).

References

[1] M. Doi, T. Kotani, and E. Takasugi, "Double beta decay and Majorana neutrino," *Progress of Theoretical Physics Supplement*, vol. 83, pp. 1–175, 1985.

[2] J. Suhonen and O. Civitarese, "Weak-interaction and nuclear-structure aspects of nuclear double beta decay," *Physics Report*, vol. 300, no. 3-4, pp. 123–214, 1998.

[3] F. T. Avignone III, S. R. Elliott, and J. Engel, "Double beta decay, Majorana neutrinos, and neutrino mass," *Reviews of Modern Physics*, vol. 80, no. 2, pp. 481–516, 2008.

[4] A. S. Barabash, "Precise half-life values for two-neutrino double-β decay," *Physical Review C*, vol. 81, no. 3, Article ID 035501, 2010.

[5] G. L. Fogli, E. Lisi, A. Marrone et al., "Global analysis of neutrino masses, mixings and phases: entering the era of leptonic CP violation searches," *Physical Review D*, vol. 86, Article ID 013012, 2012.

[6] P. A. R. Ade, N. Aghanim, C. Armitage-Caplan et al., "Planck 2013 results. XVI. Cosmological parameters," http://arxiv.org/abs/1303.5076.

[7] M. Doi and T. Kotani, "Neutrinoless modes of double beta decay," *Progress of Theoretical Physics*, vol. 89, pp. 139–159, 1993.

[8] J. Bernabeu, A. de Rujula, and C. Jarlskog, "Neutrinoless double electron capture as a tool to measure the electron neutrino mass," *Nuclear Physics B*, vol. 223, no. 1, pp. 15–28, 1983.

[9] Z. Sujkowski and S. Wycech, "Neutrinoless double electron capture: a tool to search for Majorana neutrinos," *Physical Review C*, vol. 70, no. 5, Article ID 052501, 2004.

[10] A. Aguilar-Arevalo, L. B. Auerbach, R. L. Burman et al., "Evidence for neutrino oscillations from the observation of anti-neutrino(electron) appearance in an anti-neutrino(muon) beam," *Physical Review D*, vol. 64, Article ID 112007, 2001.

[11] S. Abe, T. Ebihara, S. Enomoto et al., "Precision measurement of neutrino oscillation parameters with KamLAND," *Physical Review Letters*, vol. 100, Article ID 221803, 2008.

[12] B. Aharmin, S. N. Ahmed, J. F. Amsbaugh et al., "An independent measurement of the total active ^{8}B solar neutrino flux using an array of ^{3}He proportional counters at the Sudbury Neutrino Observatory," *Physical Review Letters*, vol. 101, Article ID 111301, 2008.

[13] A. A. Aguilar-Arevalo, C. E. Anderson, S. J. Brice et al., "Event excess in the MiniBooNE search for $\overline{\nu}_\mu \rightarrow \overline{\nu}_e$ oscillations," *Physical Review Letters*, vol. 105, no. 18, Article ID 181801, 2010.

[14] R. Wendell, C. Ishihara, K. Abe et al., "Atmospheric neutrino oscillation analysis with sub-leading effects in Super-Kamiokande I, II, and III," *Physical Review D*, vol. 81, Article ID 092004, 2010.

[15] P. Adamson, D. J. Auty, D. S. Ayres et al., "Improved search for muon-neutrino to electron-neutrino oscillations in MINOS," *Physical Review Letters*, vol. 107, Article ID 181802, 2011.

[16] Y. Abe, C. Aberle, T. Akiri et al., "Indication for the disappearance of reactor electron antineutrinos in the Double Chooz experiment," *Physical Review Letters*, vol. 108, Article ID 131801, 2012.

[17] F. P. An, J. Z. Bai, A. B. Balantekin et al., "Observation of electron-antineutrino disappearance at Daya Bay," *Physical Review Letters*, vol. 108, Article ID 171803, 2012.

[18] J. K. Ahn, S. Chebotaryov, J. H. Choi et al., "Observation of reactor electron-antineutrino disappearance in the RENO experiment," *Physical Review Letters*, vol. 108, Article ID 191802, 2012.

[19] P. Pontecorvo, "Mesonium and anti-mesonium," *Soviet Physics—Journal of Experimental and Theoretical Physics*, vol. 6, p. 429, 1957.

[20] Z. Maki, M. Nakagawa, and S. Sakata, "Remarks on the unified model of elementary particles," *Progress of Theoretical Physics*, vol. 28, pp. 870–880, 1962.

[21] P. Minkowski, "$\mu^- \rightarrow e\gamma$ at a rate of one out of 1-billion muon decays?" *Physics Letters B*, vol. 67, no. 4, pp. 421–428, 1977.

[22] T. Yanagida, "Horizontal symmetry and masses of neutrinos," in *Proceedings of the Workshop on Unified Theory and the Baryon Number in the Universe*, KEK Report 79-18, pp. 95–99, 1979.

[23] M. Gell-Mann, P. Ramond, and R. Slansky, "Complex spinors and unified theories," *CORD Conference Proceedings*, Article ID 790927, pp. 315–321, 1979.

[24] R. N. Mohapatra and G. Senjanović, "Neutrino mass and spontaneous parity nonconservation," *Physical Review Letters*, vol. 44, no. 14, pp. 912–915, 1980.

[25] J. Schechter and J. W. F. Valle, "Neutrino masses in SU(2) × U(1) theories," *Physical Review D*, vol. 22, no. 9, pp. 2227–2235, 1980.

[26] J. Beringer, J.-F. Arguin, R. M. Barnett et al., "Review of particle physics (RPP)," *Physical Review D*, vol. 86, Article ID 010001, 2012.

[27] C. Giunti and C. W. Kim, *Fundamentals of Neutrino Physics and Astrophysics*, Oxford University Press, Oxford, UK, 2007.

[28] C. Kraus, B. Bornschein, L. Bornschein et al., "Final results from phase II of the Mainz neutrino mass searchin tritium β decay," *European Physical Journal C*, vol. 40, no. 4, pp. 447–468, 2005.

[29] V. N. Aseev, A. I. Belesev, A. I. Berlev et al., "Measurement of the electron antineutrino mass in tritium beta decay in the Troitsk nu-mass experiment," *Physics of Atomic Nuclei*, vol. 75, no. 4, pp. 464–478, 2012.

[30] J. Suhonen and M. Aunola, "Systematic study of neutrinoless double beta decay to excited 0^+ states," *Nuclear Physics A*, vol. 723, pp. 271–288, 2003.

[31] J. Barea, J. Kotila, and F. Iachello, "Nuclear matrix elements for double-β decay," *Physical Review C*, vol. 87, Article ID 014315, 2013.

[32] P. K. Rath, R. Chandra, K. Chaturvedi, P. Lohani, P. K. Raina, and J. G. Hirsch, "Uncertainties in nuclear transition matrix elements for $\beta^+\beta^+$ and $\varepsilon\beta^+$ modes of neutrinoless positron double-β decay within the projected Hartree-Fock-Bogoliubov model," *Physical Review C*, vol. 87, no. 1, Article ID 014301, 2013.

[33] V. Kolhinen, V. Elomaa, T. Eronen et al., "Accurate Q value for the ^{74}Se double-electron-capture decay," *Physics Letters B*, vol. 684, no. 1, pp. 17–21, 2010.

[34] S. Eliseev, D. Nesterenko, K. Blaum et al., "Q values for neutrinoless double-electron capture in ^{96}Ru, ^{162}Er, and ^{168}Yb," *Physical Review C*, vol. 83, no. 3, Article ID 038501, 2011.

[35] M. Goncharov, K. Blaum, M. Block et al., "Probing the nuclides ^{102}Pd, ^{106}Cd, and ^{144}Sm for resonant neutrinoless double-electron capture," *Physical Review C*, vol. 84, no. 2, Article ID 028501, 2011.

[36] J. Suhonen, "Neutrinoless double beta decays of ^{106}Cd revisited," *Physics Letters B*, vol. 701, no. 4, pp. 490–495, 2011.

[37] S. Rahaman, V. Elomaa, T. Eronen et al., "Accurate Q value for the ^{112}Sn double-β decay and its implication for the search of the neutrino mass," *Physical Review Letters*, vol. 103, no. 4, Article ID 042501, 2009.

[38] D. A. Nesterenko, K. Blaum, M. Block et al., "Double-β transformations in isobaric triplets with mass numbers A = 124,130, and 136," *Physical Review C*, vol. 86, no. 4, Article ID 044313, 8 pages, 2012.

[39] V. S. Kolhinen, T. Eronen, D. Gorelov et al., "On the resonant neutrinoless double-electron-capture decay of ^{136}Ce," *Physics Letters B*, vol. 697, no. 2, pp. 116–120, 2011.

[40] S. Eliseev, C. Roux, K. Blaum et al., "Resonant enhancement of neutrinoless double-electron capture in ^{152}Gd," *Physical Review Letters*, vol. 106, no. 5, Article ID 052504, 2011.

[41] T. R. Rodríguez and G. Martínez-Pinedo, "Calculation of nuclear matrix elements in neutrinoless double electron capture," *Physical Review C*, vol. 85, no. 4, Article ID 044310, 2012.

[42] S. Eliseev, M. Goncharov, K. Blaum et al., "Multiple-resonance phenomenon in neutrinoless double-electron capture," *Physical Review C*, vol. 84, Article ID 012501, 2011.

[43] S. Eliseev, C. Roux, K. Blaum et al., "Octupolar-excitation Penning-trap mass spectrometry for Q-value measurement of double-electron capture in ^{164}Er," *Physical Review Letters*, vol. 107, no. 15, Article ID 052501, 2011.

[44] C. Droese, K. Blaum, M. Block et al., "Probing the nuclide ^{180}W for neutrinoless double-electron capture exploration," *Nuclear Physics A*, vol. 775, pp. 1–7, 2012.

[45] J. Suhonen and O. Civitarese, "Effects of orbital occupancies and spin-orbit partners on $0\nu\beta\beta$-decay rates," *Nuclear Physics A*, vol. 847, no. 3-4, pp. 207–232, 2010.

[46] J. Suhonen, "Nuclear-structure effects on double beta decays to 0^+ states in ^{76}Ge," *International Journal of Modern Physics E*, vol. 20, no. 2, pp. 451–458, 2011.

[47] J. Suhonen, "Effects of orbital occupancies and spin-orbit partners II: $0\nu\beta\beta$ decays of ^{76}Ge, ^{82}Se and ^{136}Xe to first excited 0^+ states," *Nuclear Physics A*, vol. 853, no. 1, pp. 36–60, 2011.

[48] M. Kortelainen and J. Suhonen, "Improved short-range correlations and $0\nu\beta\beta$ nuclear matrix elements of ^{76}Ge and ^{82}Se," *Physical Review C*, vol. 75, no. 5, Article ID 051303, 2007.

[49] J. Menéndez, A. Poves, E. Caurier, and F. Nowacki, "Disassembling the nuclear matrix elements of the neutrinoless $\beta\beta$ decay," *Nuclear Physics A*, vol. 818, no. 3-4, pp. 139–151, 2009.

[50] B. Crasemann, *Atomic Inner-Shell Processes*, Academic Press, New York, NY, USA, 1975.

[51] F. Šimkovic, G. Pantis, J. D. Vergados, and A. Faessler, "Additional nucleon current contributions to neutrinoless double β decay," *Physical Review C*, vol. 60, no. 5, Article ID 055502, 1999.

[52] G. A. Miller and J. E. Spencer, "A survey of pion charge-exchange reactions with nuclei," *Annals of Physics*, vol. 100, no. 1-2, pp. 562–606, 1976.

[53] H. Feldmeier, T. Neff, R. Roth, and J. Schnack, "A unitary correlation operator method," *Nuclear Physics A*, vol. 632, no. 1, pp. 61–95, 1998.

[54] M. Kortelainen, O. Civitarese, J. Suhonen, and J. Toivanen, "Short-range correlations and neutrinoless double beta decay," *Physics Letters B*, vol. 647, no. 2-3, pp. 128–132, 2007.

[55] M. Kortelainen and J. Suhonen, "Nuclear matrix elements of $0\nu\beta\beta$ decay with improved short-range correlations," *Physical Review C*, vol. 76, no. 2, Article ID 024315, 2007.

[56] J. Suhonen and M. Kortelainen, "Nuclear matrix elements for double beta decay," *International Journal of Modern Physics E*, vol. 17, no. 1, pp. 1–11, 2008.

[57] F. Šimkovic, A. Faessler, V. Rodin, P. Vogel, and J. Engel, "Anatomy of the $0\nu\beta\beta$ nuclear matrix elements," *Physical Review C*, vol. 77, no. 4, Article ID 045503, 2008.

[58] J. Suhonen, "On the double-beta decays of ^{70}Zn, ^{86}Kr, ^{94}Zr, ^{104}Ru, ^{110}Pd and ^{124}Sn," *Nuclear Physics A*, vol. 864, no. 1, pp. 63–90, 2011.

[59] J. Suhonen, "Theoretical investigation of the double-β processes in ^{96}Ru," *Physical Review C*, vol. 86, Article ID 024301, 2012.

[60] J. Suhonen, "Analysis of double-β transitions in ^{78}Kr," *Physical Review C*, vol. 87, Article ID 034318, 2013.

[61] J. Suhonen, "Double beta decays of ^{124}Xe investigated in the QRPA framework," *Journal of Physics G*, vol. 40, Article ID 075102, 2013.

[62] J. Suhonen, *From Nucleons to Nucleus: Concepts of Microscopic Nuclear Theory*, Springer, Berlin, Germany, 2007.

[63] D. S. Delion and J. Suhonen, "Microscopic description of low-lying two-phonon states: electromagnetic transitions," *Physical Review C*, vol. 67, no. 3, Article ID 034301, 2003.

[64] J. Suhonen, "Calculation of allowed and first-forbidden beta-decay transitions of odd-odd nuclei," *Nuclear Physics A*, vol. 563, no. 2, pp. 205–224, 1993.

[65] O. Civitarese and J. Suhonen, "Two-neutrino double-beta decay to excited one- and two-phonon states," *Nuclear Physics A*, vol. 575, no. 2, pp. 251–268, 1994.

[66] A. Bohr and B. R. Mottelson, *Nuclear Structure*, vol. 1, Benjamin, New York, NY, USA, 1969.

[67] J. Suhonen, T. Taigel, and A. Faessler, "pnQRPA calculation of the β^+/EC quenching for several neutron-deficient nuclei in mass regions $A = 94$–110 and $A = 146$–156," *Nuclear Physics A*, vol. 486, no. 1, pp. 91–117, 1988.

[68] J. Suhonen, "Nuclear matrix elements of $\beta\beta$ decay from β-decay data," *Physics Letters B*, vol. 607, no. 1-2, pp. 87–95, 2005.

[69] P. Vogel and M. R. Zirnbauer, "Suppression of the two-neutrino double-beta decay by nuclear-structure effects," *Physical Review Letters*, vol. 57, no. 25, pp. 3148–3151, 1986.

[70] O. Civitarese, A. Faessler, and T. Tomoda, "Suppression of the two-neutrino double β decay," *Physics Letters B*, vol. 194, no. 1, pp. 11–14, 1987.

[71] M. Baranger, "Extension of the shell model for heavy spherical nuclei," *Physical Review*, vol. 120, no. 3, pp. 957–968, 1960.

[72] T. Tomoda, "$0^+ \rightarrow 2^+$ $0\nu\beta\beta$ decay triggered directly by the Majorana neutrino mass," *Physics Letters B*, vol. 474, no. 3-4, pp. 245–250, 2000.

[73] E. Caurier, J. Menéndez, F. Nowacki, and A. Poves, "Influence of pairing on the nuclear matrix elements of the neutrinoless $\beta\beta$ decays," *Physical Review Letters*, vol. 100, no. 5, Article ID 052503, 2008.

[74] J. Suhonen and O. Civitarese, "Review of the properties of the $0\nu\beta^-\beta^-$ nuclear matrix elements," *Journal of Physics G*, vol. 39, Article ID 124005, 2012.

[75] A. S. Barabash, P. Hubert, A. Nachab, and V. Umatov, "Search for β^+EC and ECEC processes in ^{74}Se," *Nuclear Physics A*, vol. 785, no. 3-4, pp. 371–380, 2007.

[76] P. Belli, R. Bernabei, F. Cappella et al., "Search for double- β decays of ^{96}Ru and ^{104}Ru by ultra-low background HPGe γ spectrometry," *European Physical Journal A*, vol. 42, no. 2, pp. 171–177, 2009.

[77] P. Belli, R. Bernabei, F. Cappella et al., "Search for 2β decays of ^{96}Ru and ^{104}Ru by ultralow-background HPGe γ spectrometry at LNGS: final results," *Physical Review C*, vol. 87, no. 3, Article ID 034607, 8 pages, 2013.

[78] P. Belli, R. Bernabei, R. S. Boiko et al., "Search for double-β decay processes in ^{106}Cd with the help of a $^{106}CdWO_4$ crystal scintillator," *Physical Review C*, vol. 85, no. 4, Article ID 044610, 2012.

[79] A. S. Barabash, P. Hubert, A. Nachab, S. I. Konovalov, I. A. Vanyushin, and V. Umatov, "Search for β^+EC and ECEC processes in ^{112}Sn," *Physical Review C* , vol. 80, Article ID 035501, 2009.

[80] P. Belli, R. Bernabei, S. d'Angelo et al., "First limits on neutrinoless resonant 2ε captures in ^{136}Ce and new limits for other 2β

processes in ^{136}Ce and ^{138}Ce isotopes," *Nuclear Physics A*, vol. 824, no. 1–4, pp. 101–114, 2009.

[81] P. Belli, R. Bernabei, F. Cappella et al., "Search for double beta decay of zinc and tungsten with low background $ZnWO_4$ crystal scintillators," *Nuclear Physics A*, vol. 826, no. 3-4, pp. 256–273, 2009.